INTERNATIONAL JOURNAL FOR NUMERICAL AND ANALYTICAL METHODS IN GEOMECHANICS
Int. J. Numer. Anal. Meth. Geomech., **23**, 1245–1279 (1999)

PLASTICITY SOLUTIONS FOR SOIL BEHAVIOUR AROUND CONTRACTING CAVITIES AND TUNNELS

H.S. YU[1,*,†] AND R.K. ROWE[2,‡]

[1]*Department of Civil, Surveying and Environmental Engineering, The University of Newcastle, N.S.W. 2308, Australia*
[2]*Department of Civil and Environmental Engineering, The University of Western Ontario, London, Ont, Canada*

SUMMARY

The action of tunnel excavation reduces the *in-situ* stresses along the excavated circumference and can therefore be simulated by unloading of cavities from the *in-situ* stress state. Increasing evidence suggests that soil behavior in the plane perpendicular to the tunnel axis can be modelled reasonably by a contracting cylindrical cavity, while movements ahead of an advancing tunnel heading can be better predicted by spherical cavity contraction theory. In the past, solutions for unloading of cavities from *in-situ* stresses in cohesive-frictional soils have mainly concentrated on the small strain, cylindrical cavity model. Large strain spherical cavity contraction solutions with a non-associated Mohr–Coulomb model do not seem to be widely available for tunnel applications. Also, cavity unloading solutions in undrained clays have been developed only in terms of total stresses with a linear elastic-perfectly plastic soil model. The total stress analyses do not account for the effects of strain hardening/softening, variable soil stiffness, and soil stress history (OCR). The effect of these simplifying assumptions on the predicted soil behavior around tunnels is not known.

In this paper, analytical and semi-analytical solutions are presented for unloading of both cylindrical and spherical cavities from *in-situ* state of stresses under both drained and undrained conditions. The non-associated Mohr-Coulomb model and various critical state theories are used respectively to describe the drained and undrained stress-strain behaviors of the soils. The analytical solutions presented in this paper are developed in terms of large strain formulations. These solutions can be used to serve two main purposes: (1) to provide models for predicting soil behavior around tunnels; (2) to provide valuable benchmark solutions for verifying various numerical methods involving both Mohr–Coulomb and critical state plasticity models. Copyright © 1999 John Wiley & Sons, Ltd.

KEY WORDS: unloading of cavities; critical state models; plasticity; tunnelling; normally and overconsolidated clays

INTRODUCTION

Over the years, cavity expansion theory has been established as a useful tool in geotechnical engineering practice. In particular, cavity expansion solutions have been successfully used to model *in situ* soil testing (e.g. pressuremeters and cone penetrometers) and pile driving. On the other hand, cavity unloading solutions have been used as a predictive tool for modelling soil and rock behaviour around tunnels. For rock tunnels, a large number of cylindrical cavity unloading solutions have been developed for the design of tunnel support systems.[1]

* Correspondence to: H. S. Yu, Department of Civil, Surveying and Environmental Engineering, The University of Newcastle, N.S.W. 2308, Australia
† Associate Professor
‡ Professor and Chair

CCC 0363–9061/99/121245–35$17.50

Received 15 July 1998
Revised 25 November 1998

The comparative studies by Lo *et al.*[2] and Ogawa and Lo[3] indicate that, after applying a correction factor, the simple plane strain cylindrical cavity unloading solution can be satisfactorily used to predict the measured soil displacements around tunnels. Recent research carried out by Mair and Taylor[4] has highlighted the usefulness of spherical cavity unloading solutions in modelling soil behaviour around an advancing tunnel heading. After comparing the cavity unloading solutions with some field and centrifuge measurements, Mair and Taylor[4] concluded that the simple plasticity solution of the unloading of cavities can be successfully used to predict both displacements and pore pressure changes around tunnels in the clay they examined.

In the analysis of tunnels in soils, it is often important to investigate two separate cases. Firstly, the long term behavior of tunnels in cohesive frictional soils may be modelled as a fully drained problem. The drained analysis can be carried out in terms of effective stresses with the Mohr-Coulomb criterion.[5] The displacements obtained from the drained analyses include both the immediate and the time-dependent consolidation settlements. Previous cavity unloading work for modelling tunnels in Mohr–Coulomb materials has mainly concentrated on small strain, cylindrical cavity contraction models.[2,3] As noted by Mair and Taylor[4], however, for soil behaviour around an advancing tunnel heading, the unloading of a spherical cavity is more realistic. At present, it is also not clear what effects the small strain assumption used in most previous cavity models will have on the predicted soil behaviour.

Secondly, tunnel construction in clay is usually sufficiently rapid that the clay behaviour around tunnels may be assumed to be undrained. This is relevant for investigating the short-term ground settlement due to tunnelling. In the past, the analysis of undrained tunnelling has often been carried out using a total stress approach with the linear elastic-perfectly plastic Tresca model.[2,4] Despite its simplicity, the total stress approach suffers from the following drawbacks: (i) the effect of stress history (OCR) on the soil behaviour cannot be included; (ii) the variation of soil stiffness on stress level and void ratio is generally not taken into account; and (iii) the effect of soil strain-hardening/softening is not considered.

For undrained problems, a more accurate approach is to use an effective stress analysis in conjunction with well-established critical state soil models. Such an effective stress approach was used by Randolph *et al.*[6] to predict the soil behavior around driven piles. However, in this study, the finite element method had to be used. Most recently, Collins and Yu[7] have developed analytical solutions for cavity expansion in critical state soils. These newly developed analytical solutions have been used successfully to analyse soil behaviour around displacement piles in both normally and overconsolidated clays. To be useful for tunnel applications, however, analytical solutions for unloading of cavities in soils will need to be developed and this is the main purpose of the present paper.

PROBLEM DEFINITION

Following Mair and Taylor,[4] the tunnel problem to be analysed in the present paper is shown in Figure 1. It is assumed that the tunnel heading can be idealized as in Figure 1(a), where the tunnel is circular and the lining may (or may not) be installed behind the tunnel face. To simplify the mathematics of the solution, the initial stress state is assumed to be isotropic. A major assumption is that the construction of a tunnel can be modelled either in terms of the unloading of a spherical cavity (Figure 1(b)), or in terms of the unloading of a cylindrical cavity (Figure 1(c)). It is also assumed that tunnels to be analysed are constructed sufficiently deep in the ground so that the

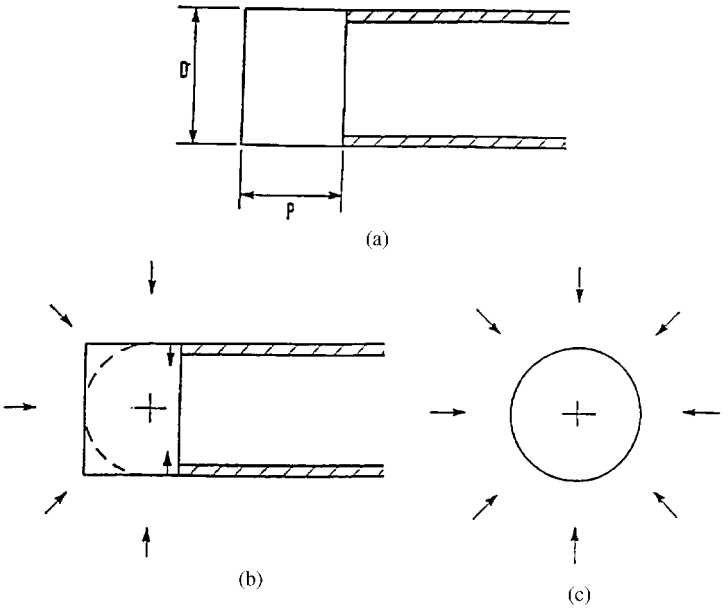

Figure 1. Idealization of a tunnel heading (after Mair and Taylor[4])

effect of free ground surface is small and can therefore be ignored. The estimate of ground surface effects may be made by using the method suggested by Sagaseta.[8]

Initially, the *in situ* stress is applied on a cavity wall (i.e. the tunnel surface). The tunnel excavation is simulated by slowly reducing the internal cavity pressure from the *in situ* value to a pressure acting on the lining (for lined tunnels) or to zero (for unlined tunnels). This paper is concerned with the displacements, stresses and pore pressure changes in the soil around tunnels at every stage of the cavity unloading process.

The objectives of this paper are:

(1) To present rigorous large strain solutions of displacements and stresses due to the unloading of both cylindrical and spherical cavities in a non-associated Mohr–Coulomb material. The solutions developed can then be used to check the accuracy of the conventional approximate small strain solutions.
(2) To develop rigorous large strain analytical solutions of displacements, stresses and pore pressure changes due to the unloading of both cylindrical and spherical cavities in critical state soils. The solutions developed can be used to account for the effects of OCR, variable soil stiffness, and strain hardening/softening.
(3) To investigate the effect of different soil models on the predicted soil behaviour; this is necessary particularly considering that there has been very little comparative research into the effect of different elastic–plastic soil models on calculated displacements due to tunnelling.[9]
(4) To conduct parametric studies to identify potentially significant factors affecting the soil displacements and stresses around the tunnel.

(5) To check the applicability of the proposed cavity unloading solutions for tunnel problems by comparing the analytical solutions with experimental data.

DRAINED SOLUTIONS

For the fully drained cases, the analysis is carried out in terms of effective stresses with drained soil strength parameters. In the past, little attention has been paid to the unloading of a spherical cavity in soils. As discussed in Brown *et al.*,[1] Ogawa and Lo[3] and Yu and Houlsby,[10] most published cavity unloading solutions were obtained for a cylindrical cavity using the small strain formulation. Because of the usefulness of the spherical cavity unloading solution in modelling soil behaviour around an advancing tunnel heading,[4] this section will present a complete large strain solution for the unloading of both cylindrical and spherical cavities in a non-associated Mohr–Coulomb material.

Equilibrium equation and stress boundary conditions

In the current configuration, the total stresses must be in equilibrium. For fully drained cases the excess pore pressure is zero and the equilibrium requirement for cavity problems can be expressed as follows:

$$\frac{\mathrm{d}\sigma'_r}{\mathrm{d}r} + k\,\frac{\sigma'_r - \sigma'_\theta}{r} = 0 \tag{1}$$

subject to the two stress boundary conditions:

$$\sigma'_r(a) = p \tag{2}$$

$$\sigma'_r(\infty) = p_0 \tag{3}$$

where a is current radius for the cavity wall, p_0 is initial mean effective stress and p is the cavity pressure. Note that the convention of compression positive is used in this paper. As in Carter *et al.*[11] and Yu and Houlsby,[10,12] the symbol k is used to denote cylindrical ($k = 1$) and spherical cavities ($k = 2$).

For cavity problems, the displacement is purely in the radial direction, which can be defined by

$$u(r) = r - r_0 \tag{4}$$

Elastic response

As a tunnel is excavated, the radial stress at the tunnel boundary decreases from the initial value of p_0. The deformation of the soil at first is purely elastic. Under conditions of radial symmetry the elastic stress–strain relationship can be expressed as

$$\dot{\varepsilon}_r = -\frac{\partial \dot{u}}{\partial r} = \frac{1}{m}\left[\dot{\sigma}'_r - \frac{k\mu}{1-\mu(2-k)}\dot{\sigma}'_\theta\right] \tag{5}$$

$$\dot{\varepsilon}_\theta = \dot{\varepsilon}_\omega = -\frac{\dot{u}}{r} = \frac{1}{m}\left[-\frac{\mu}{1-\mu(2-k)}\dot{\sigma}'_r + (1-\mu(k-1))\dot{\sigma}'_\theta\right] \tag{6}$$

where

$$m = \frac{E}{1 - \mu^2(2 - k)}$$

μ is Poisson's ratio, and E is Young's modulus. The strain in the tunnel axis for a cylindrical cavity is assumed to be zero, which is sufficient for determining the stress in that direction.[10]

The solutions of equations (5), (6) and (1) subjected to the boundary conditions (2) and (3) are well known and can be shown to be[10,11]

$$\sigma'_r = p_0 + (p - p_0)\left(\frac{a}{r}\right)^{k+1} \tag{7}$$

$$\sigma'_\theta = p_0 - \frac{(p - p_0)}{k}\left(\frac{a}{r}\right)^{k+1} \tag{8}$$

$$u = \frac{p - p_0}{2kG}\left(\frac{a}{r}\right)^{k+1} r \tag{9}$$

where G is the shear modulus. Since a compression positive notation is used in the present paper, the Mohr–Coulomb criterion for unloading of cavities is (i.e. assuming the radial stress is the minor principal stress and the hoop stress is the major principal stress):

$$\sigma'_\theta - \alpha\sigma'_r = Y \tag{10}$$

where

$$\alpha = \frac{1 + \sin\phi}{1 - \sin\phi}, \qquad Y = \frac{2c\cos\phi}{1 - \sin\phi}$$

and c and ϕ are the cohesion and the angle of internal soil friction under drained loading conditions.

It is possible that for a cylindrical cavity the assumption of the axial stress being the intermediate principal stress may violate the assumption of plane strain condition in the axial direction. As noted by Reed[13], most previous solutions have not considered this possibility and may therefore contain some inconsistency in the solutions. The sufficient condition under which the present solutions are consistent is presented in Appendix A.

As the cavity pressure p decreases further, initial yielding occurs at the cavity wall when the condition

$$p = p_1 = \frac{k + 1}{1 + \alpha k} p_0 - \frac{k}{1 + \alpha k} Y \tag{11}$$

is satisfied.

Elastic-plastic stress analysis

After initial yielding at the cavity wall, a plastic zone within the region $a \leqslant r \leqslant R$ forms around the inner wall of the cavity with the decrease of the cavity pressure p. We now consider the elastic and plastic regions of the soil separately.

Elastic region $r \geqslant R$: The stresses in the elastic zone can be obtained from (1)–(6) as follows:

$$\sigma_r' = p_0 + Br^{-(1+k)} \tag{12}$$

$$\sigma_\theta' = p_0 - \frac{B}{k} r^{-(1+k)} \tag{13}$$

where B is an integration constant.

Plastic region $a \leqslant r \leqslant R$. The stresses in the plastic zone, that must satisfy both the equilibrium equation (1) and yield function (10), can be shown to take the following form:

$$\sigma_r' = -\frac{Y}{\alpha - 1} - Ar^{k(\alpha-1)} \tag{14}$$

$$\sigma_\theta' = -\frac{Y}{\alpha - 1} - A\alpha r^{k(\alpha-1)} \tag{15}$$

where A is the second integration constant.

Continuity of stresses at the elastic–plastic interface $r = R$. The continuity of the stresses at the elastic–plastic interface can be used to determine the integration constant A and B in terms of the elastic–plastic interface radius R:

$$A = -\frac{[(\alpha-1)p_0 + Y](1+k)}{(\alpha-1)(1+k\alpha)} R^{(1-\alpha)k} \tag{16}$$

$$B = \frac{k[(1-\alpha)p_0 - Y]}{k\alpha + 1} R^{1+k} \tag{17}$$

Applying equations (14) and (16) at the cavity wall leads to a relationship between the cavity pressure p and the radius of the elastic–plastic interface R:

$$\frac{R}{a} = T^{1/k(1-\alpha)} \tag{18}$$

where

$$T = \frac{(k\alpha+1)[(\alpha-1)p + Y]}{(1+k)[(\alpha-1)p_0 + Y]} \tag{19}$$

Elastic–plastic displacement analysis

Elastic region $r \geqslant R$. The results obtained above cannot be used to calculate the distribution of stresses until the displacement field is known. Substituting equations (12), (13) and (17) into (6) leads to the displacement field in the elastic zone:

$$u = \frac{(1-\alpha)p_0 - Y}{2G(1+\alpha k)} \left(\frac{R}{r}\right)^{k+1} r \tag{20}$$

Rigorous equations for displacements in the plastic region $a \leqslant r \leqslant R$. The determination of the displacement field in the plastic zone requires the use of a plastic flow rule that indicates the relative magnitude of plastic strains in different directions.

Following Davis[14], the soil is assumed to dilate plastically at a constant rate. This non-associated flow rule with the Mohr–Coulomb yield criterion has been widely used in geotechnical engineering for modelling cohesive-frictional soil behaviour. Clearly, the use of a fixed angle of dilation is a simplification and it would be preferable to consider the angles of friction and dilation as functions of density and stress level. This would, however, require numerical methods for the solutions.[15]

The non-associated plastic flow rule in the case of cavity unloading is

$$\frac{\dot{\varepsilon}_r^p}{\dot{\varepsilon}_\theta^p} = -k\beta \tag{21}$$

where

$$\beta = \frac{1 + \sin\psi}{1 - \sin\psi}$$

and ψ is the angle of soil dilation. If $\beta = \alpha$, the plastic flow rule for the soil is said to be associated. Substituting the elastic solution for strains (5)–(6) into the plastic flow rule defined by equation (21) results in

$$\dot{\varepsilon}_r + k\beta\dot{\varepsilon}_\theta = \frac{1}{m}\left[\left(1 - \frac{k\beta\mu}{1 - \mu(2-k)}\right)\dot{\sigma}_r + \left(k\beta(1 + \mu - k\mu) - \frac{k\mu}{1 - \mu(2-k)}\right)\dot{\sigma}_\theta\right] \tag{22}$$

where m is a function of elastic material parameters defined previously. The distribution of stresses and strains in the soil at the initiation of plastic yielding can be obtained from equations (7) and (8) by putting $p = p_1$.

Following the solution procedure developed by Yu and Houlsby,[10] the integral of equation (22) from the condition at the initial yielding can be used to obtain a rigorous elastic–plastic solution for cavity unloading from the *in-situ* stress state. However, it proved to be difficult to express such a solution in closed form and instead numerical integration is needed. It is noted from the above derivation that the inclusion of elastic strains in the plastic zone has complicated the mathematics significantly. In fact, the right-hand side of equation (22) is purely due to the effect of elastic deformation in the plastic region. For soils with realistic soil properties, the value of m is very large so that the typical value of the right-hand side of (22) is generally small. If the elastic deformation in the plastic zone can be ignored, the governing equation (22) will be considerably simplified.

As in Yu and Houlsby,[10,12] the constitutive models used here are as follows. Once yielding occurs, stress–strain relationships are expressed between the Eulerian stresses (force/current area) and the logarithmic (Hencky) strains, which are simply the time integral of the deformation rates for the cavity problems in which no rotation of principal strains occurs. Of the many possible definition of large strain the Hencky definition is particularly attractive because of its simple physical interpretation for problems without rotation.

Large strain solution—neglecting elastic deformation in the plastic zone. To account for effects of large strain in the plastic zone, the logarithmic strains are adopted:

$$\varepsilon_r = -\ln\left(\frac{\mathrm{d}r}{\mathrm{d}r_0}\right) \tag{23}$$

$$\varepsilon_\theta = -\ln\left(\frac{r}{r_0}\right) \tag{24}$$

Substituting equations (23) and (24) into (22) and then ignoring the contribution of elastic deformation in the plastic zone result in the following large strain displacement equation:

$$r^{k\beta}\mathrm{d}r = r_0^{k\beta}\mathrm{d}r_0 \tag{25}$$

which can be integrated from the elastic–plastic interface to any point in the plastic zone leading to

$$r^{1+k\beta} - R^{1+k\beta} = r_0^{1+k\beta} - R_0^{1+k\beta} \tag{26}$$

As R can be linked to R_0 by the elastic solution (20), equation (26) actually defines the displacement field in the plastic region.

At the cavity wall, equation (26) reduces to

$$a^{1+k\beta} - a_0^{1+k\beta} = R^{1+k\beta} - R_0^{1+k\beta} \tag{27}$$

With the aid of equation (18), the displacement at cavity wall can be linked to the cavity pressure as follows:

$$\frac{1-(a_0/a)^{1+k\beta}}{1-(R_0/R)^{1+k\beta}} = T^{(1+k\beta)/(k(1-\alpha))} \tag{28}$$

where T is a function of cavity pressure p as defined by equation (19)

Small strain solution—neglecting elastic deformation in the plastic zone. After ignoring the elastic deformations in the plastic zone, the usual small-strain definition for both radial and hoop strains can be substituted into equation (22) to integrate to give

$$\frac{\mathrm{d}u}{\mathrm{d}r} + k\beta\frac{u}{r} = 0 \tag{29}$$

which has the general solution

$$u = -\frac{C}{r^{k\beta}} \tag{30}$$

With the known displacement at $r = R$ from equation (20), the constant C can be obtained as

$$C = -\frac{(1-\alpha)p_0 - Y}{2G(1+\alpha k)}R^{1+k\beta} \tag{31}$$

Substituting (31) back into (30) gives the displacement field in the plastic zone:

$$u = \frac{(1-\alpha)p_0 - Y}{2G(1+\alpha k)}\left(\frac{R}{r}\right)^{1+k\beta} r \tag{32}$$

As a special case, the displacement at the cavity wall can be obtained by putting $r = a$ in (32):

$$\frac{a-a_0}{a} = \frac{(1-\alpha)p_0 - Y}{2G(1+\alpha k)} T^{(1+k\beta)/k(1-\alpha)} \tag{33}$$

UNDRAINED SOLUTIONS

The undrained solution for cavity unloading problems developed in this section follows closely the loading analysis of Collins and Yu.[7]

Kinematics of cavity unloading

The constant-volume condition under undrained loading conditions gives the following relation between r, the current radius of a material element which was initially at r_0 and the current and initial radii of the cavity – a and a_0, respectively:

$$r_0^{k+1} - r^{k+1} = a_0^{k+1} - a^{k+1} \tag{34}$$

The radial speed of the element is hence related to the speed of contraction of the cavity by

$$w = \dot{r} = \left(\frac{a}{r}\right)^k \dot{a} \tag{35}$$

so that the radial, circumferential, shear and volumetric strain rates can be expressed as follows:

$$\dot{\varepsilon}_r = -\frac{\partial w}{\partial r} = \left[\frac{k a^k}{r^{k+1}}\right]\dot{a} \tag{36}$$

$$\dot{\varepsilon}_\theta = -\frac{w}{r} = -\left[\frac{a^k}{r^{k+1}}\right]\dot{a} \tag{37}$$

$$\dot{\gamma} = \dot{\varepsilon}_r - \dot{\varepsilon}_\theta = \left[(k+1)\frac{a^k}{r^{k+1}}\right]\dot{a} \tag{38}$$

$$\dot{\delta} = \dot{\varepsilon}_r + k\dot{\varepsilon}_\theta = 0 \tag{39}$$

Using equation (34) the shear strain rate can also be written in terms of the initial position of the particle r_0:

$$\dot{\gamma} = \left[\frac{(k+1)a^k}{(a^{k+1} + r_0^{k+1} - a_0^{k+1})}\right]\dot{a} \tag{40}$$

Since r_0 is fixed for a given particle, equation (40) can be integrated to give the finite Lagrangean shear strain:

$$\gamma = \ln\left(\frac{(a^{k+1} + r_0^{k+1} - a_0^{k+1})}{r_0^{k+1}}\right) = (k+1)\ln\frac{r}{r_0} \tag{41}$$

associated with the particle originally at r_0. This relation can now be written back in terms of r, the current co-ordinate of the particle:

$$\dot{\gamma} = -\ln\left[1 - \frac{(a^{k+1} - a_0^{k+1})}{r^{k+1}}\right] \tag{42}$$

or inversely

$$\gamma^{k+1} = \frac{a_0^{k+1} - a^{k+1}}{\exp(-\gamma) - 1} \tag{43}$$

by using (34) to eliminate r_0. This expression gives the distribution of shear strain with radius r at the instant when the current cavity radius is a.

From (41)–(43), it follows that the relations between radial and shear strain increments (i) for a given particle and (ii) at a fixed instant of time are, respectively,

$$(k+1)\frac{\mathrm{d}r}{r} = \mathrm{d}\gamma \quad \text{and} \quad (k+1)\frac{\mathrm{d}r}{r} = -\frac{d\gamma}{\exp(\gamma) - 1} \tag{44}$$

Note that at the cavity wall the shear strain is

$$\gamma_c = (k+1)\ln\frac{a}{a_0} \tag{45}$$

which is infinite when the initial cavity radius is zero. These results are kinematic and apply in both the elastic and elastic/plastic phases of the cavity contraction.

Elastic unloading

As in Collin and Yu,[7] the following deviator and mean effective stresses are used for the analysis of cavity unloading problems:

$$q = \sigma_r' - \sigma_\theta' \quad \text{and} \quad p' = \frac{\sigma_r' + k\sigma_\theta'}{1+k} \tag{46}$$

where σ_r' and σ_θ' are the effective radial and hoop stresses, respectively. It is noted that for the cylindrical case the above definitions for deviator and mean effective stresses do not depend on the axial stress, and therefore are slightly different from the usual 3D definitions used in critical state soil mechanics.[16,17,18] The chief reason for using the above definitions in this paper is to simplify the mathematical derivation so that closed form solutions are made possible. A recent finite element study with 3D critical state models by Sheng *et al.*[19] suggests that the error due to the use of the simplified definitions (46) is negligible for the analysis of cylindrical cavity problems.

To fully take account of the scaling laws it is convenient to non-dimensionalize all stresses and moduli by some representative stress. Such non-dimensional variables will be denoted by

superposed bars. Here we adopt the usual convention in critical state soil mechanics and use the equivalent consolidation pressure p'_e as this representative pressure. The elastic constitutive law is most conveniently expressed in rate form:

$$\dot{\delta}^e = \frac{\mathring{\bar{p}}'}{\bar{K}(\bar{p}', v)} \quad \text{and} \quad \dot{\gamma}^e = \frac{\mathring{\bar{q}}}{2\bar{G}(\bar{p}', v)} \tag{47}$$

where $\dot{\delta}^e$ and $\dot{\gamma}^e$ represent the elastic volumetric and shear strain rates respectively; $\mathring{\bar{p}}'$ and $\mathring{\bar{q}}$ are the material rates of change of the non-dimensional, effective mean and shear stress invariants. The instantaneous bulk and shear moduli are both functions of the specific volume v and mean effective pressure p' in general, so that the elastic stress–strain relation obtained by integration will be non-linear. The symbol $\mathring{(\ )}$ denotes the material time derivative associated with a given solid material particle and it is related to the local time derivative $\dot{(\ )}$, evaluated at fixed position r, by

$$\mathring{(\ )} = \dot{(\ )} + w\frac{\partial()}{\partial r} \tag{48}$$

where w is the radial speed of a solid material element.

In the initial, purely elastic phase of an undrained expansion the elastic volumetric strain rate $\dot{\delta}^e = 0$, so that from equation (47) the effective mean pressure remains constant and is equal to its initial value p'_0. The instantaneous elastic bulk and shear moduli hence also remain constant and equal to their initial values K_0 and G_0, respectively. The second part of equation (47) for the elastic shear strain rate can be integrated along a particle path, so that the shear stress invariant q is just twice the initial elastic shear modulus times the finite shear strain γ, viz.,

$$\gamma = \frac{\bar{q}}{2\bar{G}_0} < 0 \tag{49}$$

The radial and circumferential components of effective stress are hence given by

$$\bar{\sigma}'_r = \bar{p}'_0 + \frac{2\bar{G}_0\gamma k}{k+1} \quad \text{and} \quad \bar{\sigma}'_\theta = \bar{p}'_0 - \frac{2\bar{G}_0\gamma}{k+1} \tag{50}$$

These stresses can now be expressed in terms of the radial position co-ordinates by eliminating γ using either (41) or (42).

The effective stress distributions have been found without reference to the equilibrium equations and without the need to make any small strain assumptions. Since the effective mean pressure is constant the stress path of a material element in this elastic phase of the contraction is a vertical line in the $\bar{q}$–$\bar{p}'$ diagram (Figure 2).

The soil first goes plastic at the cavity wall, when the shear stress invariant reaches the yield value q_0, which will depend upon the particular yield criterion. The corresponding shear strain is

$$\gamma_0 = (k+1)\ln\frac{a_1}{a_0} = \frac{\bar{q}_0}{2\bar{G}_0} = \frac{q_0}{2G_0} \tag{51}$$

where a_1 is the cavity radius at the onset of yielding, γ_0 is the shear strain to yield and is a measure of the compliance of the material. In a perfectly plastic model $q_0 = -2s_u$ where s_u is the undrained shear strength.

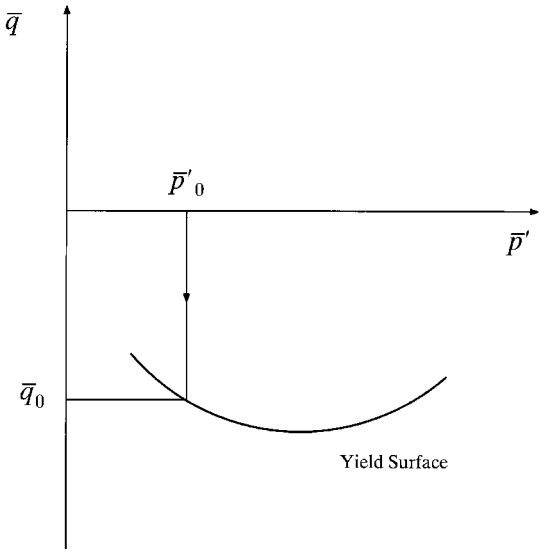

Figure 2. Stress path for elastic phase of cavity unloading

These results are also valid in the outer elastic region during the elastic–plastic phase of the contraction. The radius of the elastic/plastic boundary R at the instant when the cavity has radius a is given by

$$\left(\frac{R}{a}\right)^{k+1} = \frac{1-(a_0/a)^{k+1}}{1-\exp(-\gamma_0)} \tag{52}$$

using (42) or (43), this relation between the shear strain and radial co-ordinate can alternatively be written as

$$\left(\frac{r}{R}\right)^{k+1} = \frac{\exp(-\gamma_0)-1}{\exp(-\gamma)-1} \tag{53}$$

Elastic-plastic unloading

Effective stress distributions. In this section, the basic solution is developed in a general form appropriate to a wide class of materials, where the yield condition and plastic flow rule can be written in the form

$$\bar{q} = f(\bar{p}') \quad \text{and} \quad \frac{\dot{\delta}^{\mathrm{p}}}{\dot{\gamma}^{\mathrm{p}}} = g(\bar{p}'). \tag{54}$$

In an undrained deformation the total volumetric strain rate is zero, so that $\dot{\delta}^{\mathrm{e}} = -\dot{\delta}^{\mathrm{p}}$. It follows from (47) and (54) that the total strain rate is

$$\dot{\gamma} = \dot{\gamma}^{\mathrm{e}} + \dot{\gamma}^{\mathrm{p}} = L(\bar{p}')\overset{\circ}{\bar{p}} \tag{55}$$

where

$$L(\bar{p}') = \frac{f'(\bar{p}')}{2\bar{G}(\bar{p}')} - \frac{1}{\bar{K}(\bar{p}')\, g(\bar{p}')} \tag{56}$$

Integrating (55) along a particle path starting at the elastic–plastic boundary gives a relation between the finite shear strain and the effective mean pressure:

$$\gamma = \gamma_0 + I(\bar{p}') - I(\bar{p}'_0) \tag{57}$$

where

$$I(\bar{p}') = \int^{\bar{p}'} L(\bar{p}')\, \mathrm{d}\bar{p}' \tag{58}$$

As a special case, (57) describes the relationship between the cavity pressure and the cavity shear strain after the cavity wall becomes plastic. As will be shown in a later section the integral (58) can be evaluated analytically for the original Cam-Clay model and is readily evaluated numerically in other cases. The variation of $\bar{p}'$ with radius r can be obtained implicitly by eliminating γ between (57) and (41), (42) or (53).

Calculation of excess pore pressures. The distribution of pore pressure $U(r)$ can be calculated from the quasi-static radial equilibrium equation in terms of total stresses:

$$\frac{\mathrm{d}\bar{\sigma}_r}{\mathrm{d}r} + k\frac{\bar{\sigma}_r - \bar{\sigma}_\theta}{r} = 0 \tag{59}$$

Since $\bar{\sigma}_r = \bar{p} + (k/(k+1))\,\bar{q}$ and $\bar{p} = \bar{U} + \bar{p}'$, the non-dimensional pore pressure gradient is given by

$$\frac{\mathrm{d}\bar{U}}{\mathrm{d}r} = -\frac{\mathrm{d}\bar{p}'}{\mathrm{d}r} - \frac{k}{k+1}\frac{\mathrm{d}\bar{q}}{\mathrm{d}r} - \frac{k\bar{q}}{r} \tag{60}$$

Since the effective mean stress distribution is constant in the elastic region, the change in the pore pressure (i.e. excess pore pressure) in the elastic zone is given by

$$\Delta\bar{U} = -\frac{k}{k+1}\bar{q} - k\int \bar{q}\frac{\mathrm{d}r}{r} \tag{61}$$

Bur $\bar{q}$ and $(\mathrm{d}r/r)$ can both be expressed in terms of γ from (49) and the second equation of (44), so that (61) becomes

$$\Delta\bar{U} = -\frac{2k\bar{G}_0}{k+1}\left[\gamma - \int_0^\gamma \frac{\gamma}{\exp(\gamma) - 1}\mathrm{d}\gamma\right] \doteq -\frac{k\bar{G}_0\gamma^2}{2(k+1)} \tag{62}$$

The excess pore pressure at the elastic–plastic boundary is therefore

$$\Delta\bar{U}_0 = -\frac{k\bar{G}_0\gamma_0^2}{2(k+1)} \tag{63}$$

Excess pore pressures in the plastic region. Integrating (60) through the plastic region from the elastic/plastic boundary yields a relation between the excess pore pressure and the finite shear strain:

$$\Delta\bar{U} = \Delta\bar{U}_0 - (\bar{p}' - \bar{p}'_0) - \frac{k}{k+1}(\bar{q} - \bar{q}_0 - J) \tag{64}$$

where the integral J is most conveniently evaluated numerically by expressing both $\bar{q}$ and r in terms of $\bar{p}$ using (44), (54) and (55):

$$J = \int_{\gamma_0}^{\gamma} \frac{\bar{q}}{(\exp(\gamma) - 1)} \mathrm{d}\gamma = \int_{\bar{p}'_0}^{\bar{p}'} \frac{f(\bar{p}')\, L(\bar{p}')}{\exp(\gamma) - 1} \mathrm{d}\bar{p}' \tag{65}$$

Again, as a special case, (64) represents the plastic relationship between the excess pore pressure and the finite shear strain for the cavity wall. Once the effective stress has essentially reached the critical rate, the value of $\bar{q}$ is effectively constant and (65) can then be integrated analytically to give

$$J \doteq \bar{q}_{\mathrm{cs}} \ln \frac{\exp(-\gamma) - 1}{\exp(-\gamma_0) - 1} \tag{66}$$

Special case: linear elastic–perfectly plastic tresca model

Before discussing the solutions for various critical state models it is useful to firstly derive the solution for a perfectly plastic Tresca model. This corresponds to the situation when the *in situ* soil under undrained loading conditions behaves purely elastically before reaching the critical state. Since the shear stress and effective mean pressure are now constant through the plastic annulus the J integral in (65) can be evaluated analytically, giving

$$\Delta\bar{U} = \Delta\bar{U}_0 + \frac{k}{k+1} \bar{q}_{\mathrm{cs}} \ln \frac{\exp(-\gamma) - 1}{\exp(-\gamma_0) - 1} \tag{67}$$

or, in terms of the radial co-ordinate

$$\Delta\bar{U} = \Delta\bar{U}_0 + k\bar{q}_{\mathrm{cs}} \ln \frac{R}{r} = \Delta\bar{U}_0 + \frac{k}{k+1} \bar{q}_{\mathrm{cs}} \ln \frac{(a_0/r)^{k+1} - (a/r)^{k+1}}{\exp(-\gamma_0) - 1} \tag{68}$$

using (52) and (53). To first order in the elastic limit strain γ_0 the excess pore pressure at the cavity wall is

$$\Delta\bar{u}_{\mathrm{c}} \doteq \frac{k}{k+1} \bar{q}_{\mathrm{cs}} \left[\ln \left(\left(\frac{a_0}{a} \right)^{k+1} - 1 \right) + \ln I_r \right] \tag{69}$$

note $I_r = G/s_{\mathrm{u}}$ is the rigidity index; s_{u} is undrained shear strength. Using the above equation, the total radial stress solution at the cavity wall can be derived:

$$\bar{\sigma}_r|_{\mathrm{c}} = \bar{p}_0 + \frac{k}{k+1} \bar{q}_{\mathrm{cs}} \left[1 + \ln \left(\left(\frac{a_0}{a} \right)^{k+1} - 1 \right) + \ln \frac{G}{s_{\mathrm{u}}} \right] \tag{70}$$

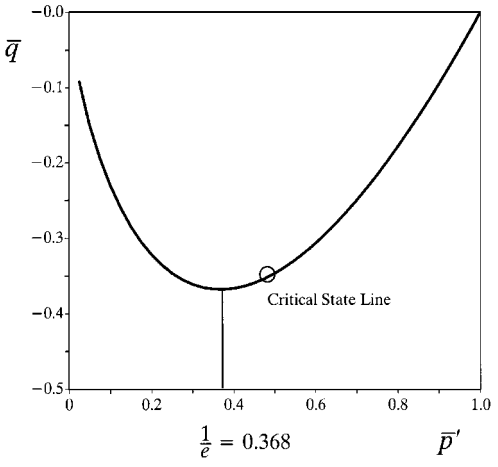

Figure 3. The original Cam-Clay yield surface for cavity unloading

with $q_{cs} = -2s_u$ the above equation can be reduced to the following cavity pressure-contraction relationship:

$$p = p_0 - \frac{2ks_u}{1+k}\left[1 + \ln\frac{G}{s_u}\right] - \frac{2ks_u}{1+k}\ln\left[\left(\frac{a_0}{a}\right)^{k+1} - 1\right] \tag{71}$$

where p is the total cavity pressure and p_0 is the initial total stress in the soil.

For a complete unloading cavity which is relevant for unlined tunnels, the maximum displacement at the cavity wall is obtained by setting $p = 0$ in equation (71):

$$\frac{a_0}{a} = \left[1 + \exp\left(\frac{1+k}{2k} \times \frac{p_0}{s_u} - 1 - \ln\frac{G}{s_u}\right)\right]^{1/(k+1)} \tag{72}$$

Critical state soil plasticity models

The original Cam-Clay model for both normally and overconsolidated clays. The original Cam-Clay model was proposed by Schofield and Wroth[16] to describe the stress–strain behaviour of clays. The yield surface of this model for cavity unloading problems can be shown to be

$$\bar{q} = f(\bar{p}') = \frac{M}{\Lambda}\bar{p}' \ln \bar{p}' \tag{73}$$

where the stresses have been non-dimensionalized by the equivalent consolidation pressure at the same specific volume v:

$$p'_e = \exp\left(\frac{N - v}{\lambda}\right) \tag{74}$$

The constant $\Lambda = 1 - \kappa/\lambda$, where κ, λ are the slopes of the elastic swelling line and normal consolidation line, respectively, in $\ln p' - v$ space and N is the value of v on the normal consolidation line when $p' = 1$ kPa. The final critical state constant M is the slope of the critical state line in $\bar{p}'$–$\bar{q}$ space. The original Cam-Clay yield surface defined in (73) is shown in Figure 3.

In this model the elastic moduli are given by

$$\bar{K} = \frac{v\bar{p}'}{\kappa} \quad \text{and} \quad \bar{G} = \frac{(1+k)(1-2\mu)}{2(1+(k-1)\mu)}\bar{K} \tag{75}$$

where μ denotes Poisson's ratio. Some authors assume μ to be constant whilst others keep G fixed and use (75) to calculate Poisson's ratio.[17] For comparison, it will be demonstrated in the next section that a constant shear modulus can also be incorporated in the present cavity unloading solution procedure.

The overconsolidation ratio (OCR) in terms of the mean effective stress is

$$n_p = (\bar{p}'_0)^{-1/\Lambda} \tag{76}$$

At the critical state $\bar{q}/\bar{p}' = M$, $n_p = e = 2{\cdot}718$ and $\bar{p}' = \mathrm{e}^{-\Lambda}$, whilst the undrained stress path in $\bar{p}'$–$\bar{q}$ space has a maximum value when $\bar{p}' = 1/e = 0{\cdot}368$ and $\bar{q}/\bar{p}' = M/\Lambda$ as shown in Figure 3. The ratio of the plastic volumetric and shear strain rates calculated from the normal flow rule is

$$\frac{\dot{\delta}^{\mathrm{p}}}{\dot{\gamma}^{\mathrm{p}}} = g(\bar{p}') = -\frac{kM}{(k+1)\Lambda}(\Lambda + \ln \bar{p}') \tag{77}$$

The function $L(\bar{p}')$ needed to calculate the effective pressure distributions in (56) is hence

$$L(\bar{p}') = \frac{A(1+\ln \bar{p}')}{\bar{p}'} + \frac{B}{\bar{p}'(\Lambda + \ln \bar{p}')} \tag{78}$$

and upon integration the function needed in (57) to calculate the shear strain is

$$I(\bar{p}') = A(\ln \bar{p}' + \tfrac{1}{2}(\ln \bar{p}')^2) + B \ln|(\Lambda + \ln \bar{p}')| \tag{79}$$

where $\mathrm{A} = M\kappa/(2\Lambda\alpha v)$ and $B = (k+1)\Lambda\kappa/(kMv)$ are constants. Note that the value of the integral I and hence the shear strain is inversely proportional to the specific volume v.

The original Cam-Clay model for normally consolidated and lightly overconsolidated clays—The Hvorslev yield surface for heavily overconsolidated clays. It is well established that the original Cam-Clay yield surface overpredicts the soil strength significantly for heavily overconsolidated clays. In this case, the Hvorslev surface has often been used as the yield function. The Hvorslev yield surface is a straight line in $\bar{p}'$–$\bar{q}$ space[18]

$$\bar{q} = -h\bar{p}' - (M-h)\exp(-\Lambda) \tag{80}$$

where h is the slope of the Hvorslev yield surface (Figure 4).

It is also noticed that the use of (75) for heavily overconsolidated clays would result in unrealistically low values of the elastic moduli. To overcome this limitation, Randolph *et al.*[6] proposed a more realistic hypothesis that is to select G as half of the maximum value of the elastic bulk modulus, $K_{\max}$ that was ever reached during the stress history of the soil. In their proposal, the bulk modulus is still assumed to be pressure dependent, and so the resulting model is conservative for elastic behaviour (see Reference 20). Equation (75) is hence replaced by the

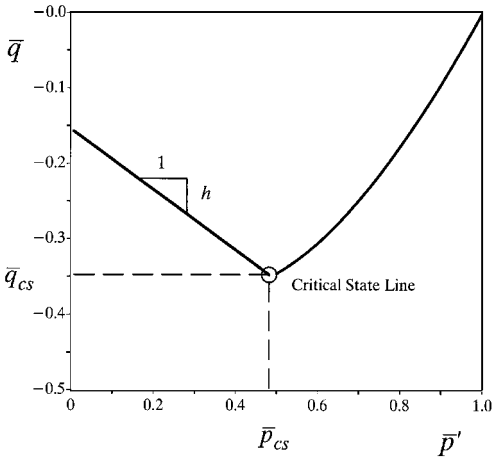

Figure 4. The original Cam-Clay-Hvorslev yield surface for cavity unloading

following expression for heavily overconsolidated clays:

$$\bar{K} = \frac{v\bar{p}'}{\kappa} \quad \text{and} \quad \bar{G} = \frac{v + \lambda(\Lambda - 1)\ln n_p}{2\kappa}(n_p)^{1-\Lambda} \tag{81}$$

Using (80) as the yield function, (73) as the plastic potential and (81) for the elastic moduli, we can obtain

$$L(\bar{p}') = -\frac{h}{2\bar{G}} + \frac{(1+k)\kappa}{kv(M-h)}\frac{1}{(\bar{p}' - \exp(-\Lambda))} \tag{82}$$

and

$$I(\bar{p}') = -\frac{h\bar{p}'}{2\bar{G}} + \frac{(1+k)\kappa}{kv(M-h)}\ln(\bar{p}' - \exp(-\Lambda)) \tag{83}$$

where the constant $\bar{G}$ is given by equation (81). Therefore the plastic flow rule in this case is non-associated.

The modified Cam-Clay model for both normally and overconsolidated clays. To improve the performance of the original Cam-Clay model for normally consolidated clays, Roscoe and Burland[21] proposed the modified Cam-Clay model. The modified Cam-Clay yield surface for cavity unloading problems is

$$\bar{q} = f(\bar{p}') = -M\bar{p}'\sqrt{(\bar{p}'^{-1/\Lambda} - 1)} \tag{84}$$

At the critical state $\bar{q}/\bar{p}' = M$, $n_{\mathrm{p}} = 2$ and $\bar{p}' = 2^{-\Lambda}$, as shown in Figure 5.

The ratio of the plastic volumetric and shear strain rates calculated from the normal flow rule is

$$\frac{\dot{\delta}^{\mathrm{p}}}{\dot{\gamma}^{\mathrm{p}}} = g(\bar{p}') = \frac{k}{(k+1)}\left(\frac{M^2 - \eta^2}{2\eta}\right) \tag{85}$$

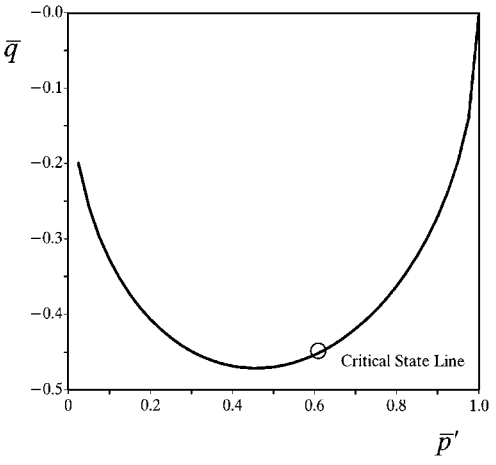

Figure 5. The modified Cam-Clay yield surface for cavity unloading

where η can be expressed as a function of mean effective stress using (84). The function $L(\bar{p}')$ needed to calculate the effective pressure distributions in (56) can be obtained by using (84) and (85). Unlike the original Cam-Clay model, the function needed in (58) to calculate the shear strain for the modified Cam-Clay model cannot be obtained in closed form and instead a simple numerical integration must be used.

NUMERICAL RESULTS

Soil behaviour around tunnels in fully drained cohesive-frictional soils

Some selected results of soil behaviour around tunnels in a Mohr–Coulomb material with a friction angle of $\phi' = 40^\circ$, a cohesion parameter of $Y/p_0 = 1{\cdot}0$ and a Poisson's ratio of 0·3 are presented in this subsection. The effect of soil dilatancy on the predicted soil behaviour around tunnels is studied by using three dilation angles of 0, 20 and 40°. It is true that the high values chosen for the angles of internal friction and dilation may not be encountered in practice for cohesive-frictional soils, and the reason for using these high values for example calculations is to illustrate the maximum possible effects of soil strength and dilatancy on soil behaviour around tunnels.

The cavity contraction curves (i.e. the ground response curves as referred to by Brown *et al.*[1]) and soil displacement distribution at the instant of complete unloading (i.e. the cavity pressure is reduced to zero and this is the case for unlined tunnelling) for the case of $G/p_0 = 10$ are plotted in Figures 6–8. A low value of stiffness index G/p_0 is selected to investigate the difference between small strain and large strain formulations. For comparison, solutions for both cylindrical and spherical cavities are presented together.

Based on the results shown in Figures 6–8, the following observations can be made:

(a) The small difference between solutions from both small and large-strain formulations shown in Figures 6–8 suggests that for tunnelling problems the small-strain solutions would be adequate for practical purposes.

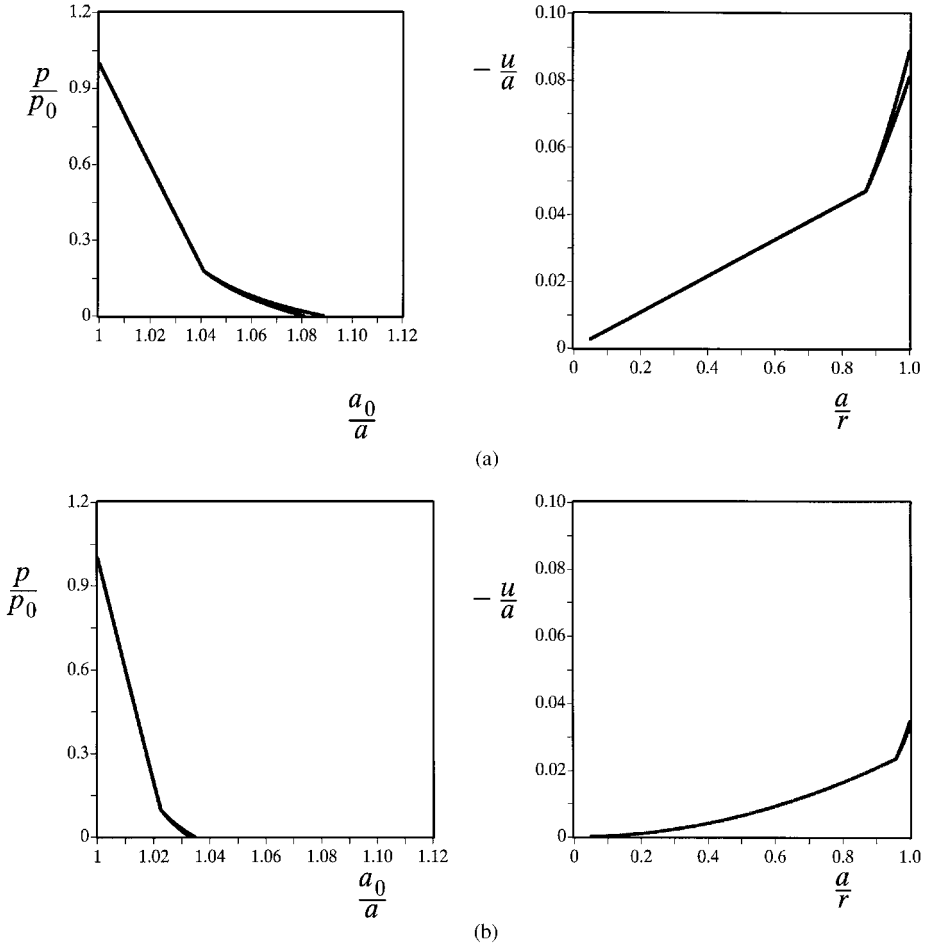

Figure 6. Soil behaviour around tunnels in drained Mohr–Coulomb soils using both small and large strain solutions ($\phi = 40^\circ$, $\psi = 40^\circ$, $Y/p_0 = 1{\cdot}0$, $G/p_0 = 10$), (a) cylindrical cavity model; (b) spherical cavity model

(b) The soil displacements induced by tunnelling from the plane strain cylindrical cavity theory is about twice as large as those from the spherical cavity theory.
(c) In the elastic region, the cylindrical cavity theory predicts that the normalized displacement $-u/a$ varies linearly with a/r. It is interesting to note that in the plastic region, the variation may also be assumed to be linear. However, the slope of the displacement variation in the plastic zone is much larger than that in the elastic zone.
(d) The soil displacements induced by tunnelling increase with increasing dilation angle. Also the size of plastic zone increases when the value of dilation angle is increased.

To investigate the effect of soil stiffness index G/p_0 on the predicted soil behaviour, the stiffness index value is changed from 10 to 50. The results for the stiffness index of 50 are given in Figure 9. By comparing Figure 9 with Figure 7, it can be seen easily that the ground response curves and soil displacements are very sensitive to the value of soil stiffness. In fact, by increasing

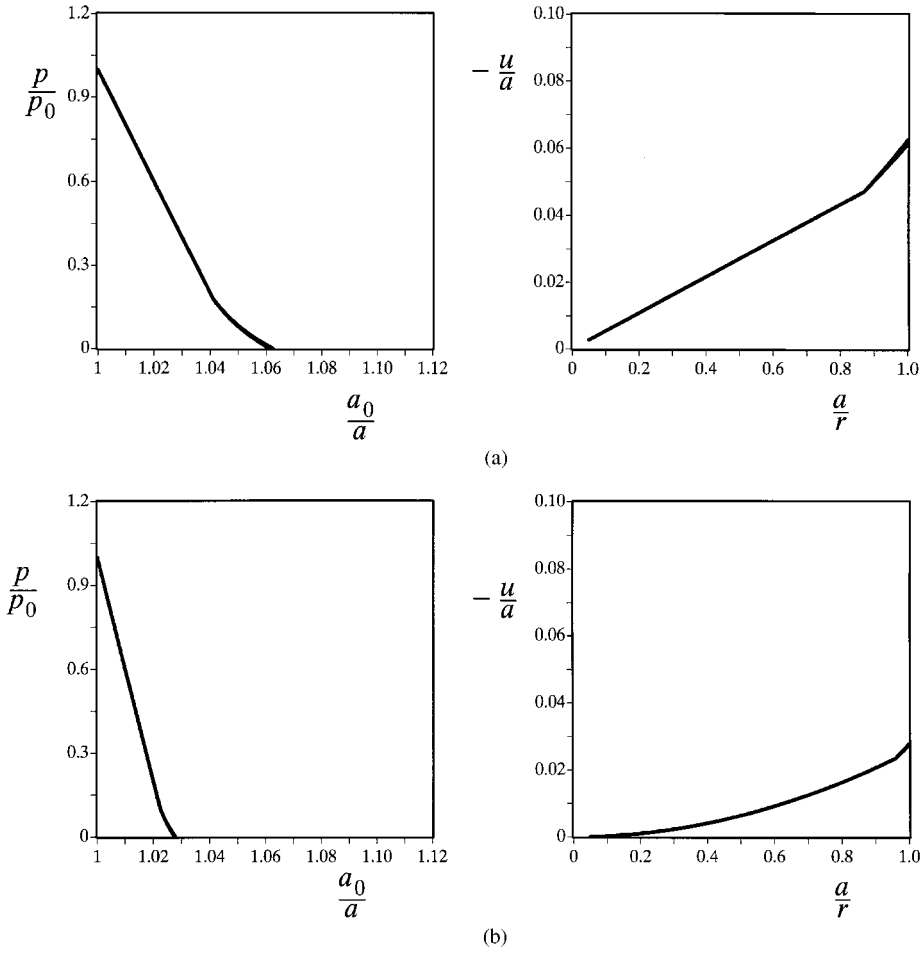

Figure 7. Soil behaviour around tunnels in drained Mohr–Coulomb soils using both small- and large-strain solutions ($\phi = 40^\circ$, $\psi = 20^\circ$, $Y/p_0 = 1{\cdot}0$, $G/p_0 = 10$), (a) cylindrical cavity model; (b) spherical cavity model

the stiffness index from 10 to 50, the soil displacements due to tunnelling are reduced by about five times.

In addition to the ground response curves and displacement distributions, the solutions for stresses have also been obtained in the present paper. Plotted in Figure 10 are the effective stress distributions around tunnels in a Mohr–Coulomb material at the instant of complete unloading. Once again, solutions for both cylindrical and spherical cavities are given.

Soil behaviour around tunnels in undrained clay

In this subsection, selected results of soil behaviour around tunnels in undrained clays are presented by using various critical state models. The values of the critical state parameters chosen for the examples presented here are those relevant to London clay: $\Gamma = 2{\cdot}759$, $\lambda = 0{\cdot}161$,

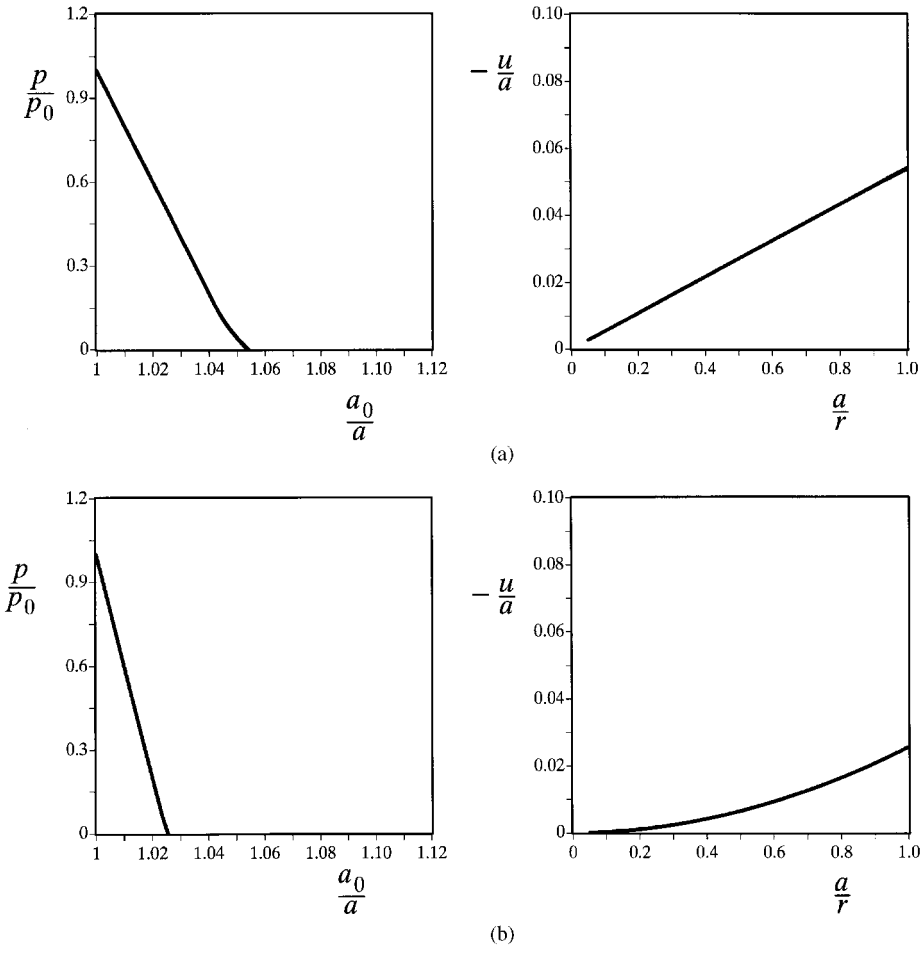

Figure 8. Soil behaviour around tunnels in drained Mohr–Coulomb soils using both small- and large strain solutions ($\phi = 40^\circ$, $\psi = 0^\circ$, $Y/p_0 = 1{\cdot}0$, $G/p_0 = 10$), (a) cylindrical cavity model; (b) spherical cavity model

$\kappa = 0{\cdot}062$, the critical state fraction angle $\phi'_{cs} = 22{\cdot}75^\circ$ and the Hvorslev friction angle $\phi'_{hc} = 19{\cdot}7^\circ$.[16,22] All the results presented are for the case when the specific volume of the soil v is equal to 2·0. The Poisson's ratio μ is assumed to be 0.3 when the original and modified Cam-Clay models are used. If the critical state friction angle of the soil is assumed to be the same for both the triaxial and plane strain loading conditions Reference 22, p. 178, for experimental evidence and further discussion), the values of M for both spherical and cylindrical cavities can be determined using $M = 6 \sin \phi'_{cs}/(3 - \sin \phi'_{cs})$ and $M = 2 \sin \phi'_{cs}$, respectively. Similar expressions can be used to determine h from ϕ'_{hc}. The vertical effective stress σ'_z for the cylindrical case can be obtained by following Yu and Houlsby.[10] For convenience, the initial soil parameters (i.e. the ratio of shear strength to initial mean effective stress and initial stiffness index) for the analyses presented in Figures 11–18 are summarized in Table I.

The first set of results is obtained with the original Cam-Clay model. Results showing the cavity contraction curves (including both the cavity pressure and the pore pressure change) and

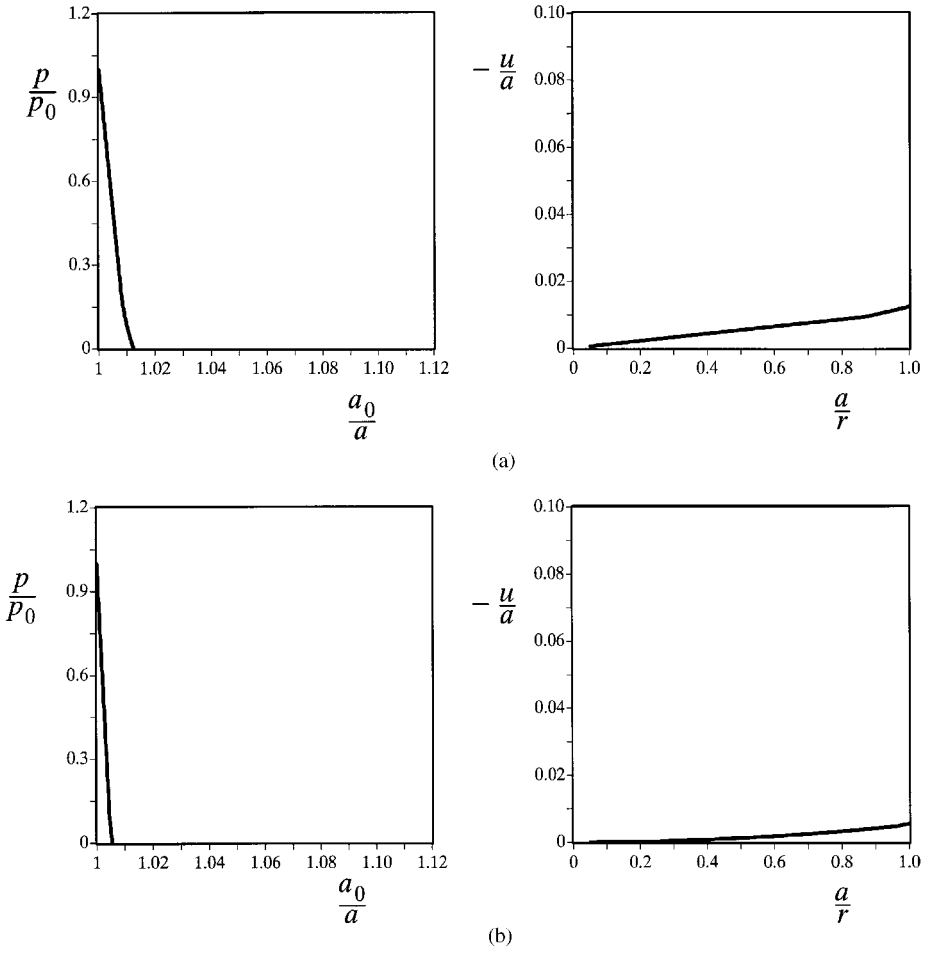

Figure 9. Soil behaviour around tunnels in drained Mohr–Coulomb soils for ($\phi = 40°$, $\psi = 20°$, $Y/p_0 = 1{\cdot}0$, $G/p_0 = 50$), (a) cylindrical cavity model; (b) spherical cavity model

displacement distribution at the instant of compete unloading for the overconsolidation ratios of $n_p = 1{\cdot}001$, 2·0, 5·0. 10·0 are presented in Figures 11–14. The reason for using $n_p = 1{\cdot}001$ to represent a normally consolidated clay is that when $n_p = 1$ the shear strain required to reach the yield surface γ_0 is zero and from equation (52) the radius of the elastic–plastic boundary becomes indeterminate. All the stresses and pressures have been normalized by the undrained shear strength of the soil which is defined by $s_u = 0{\cdot}5M \exp((\Gamma - v)/\lambda)$. It is noted that the total radial stress values presented in the section do not include ambient pore pressure.

The following conclusions can be drawn from the large-strain solutions presented in Figures 11–14:

(a) For normally consolidated clays, when the cavity pressure is reduced the pore pressure increases initially before eventually decreasing to a much lower value. On the other hand, for both lightly and heavily overconsolidated clays, the pore pressure remains constant during the elastic unloading before starting to decrease when unloading become plastic.

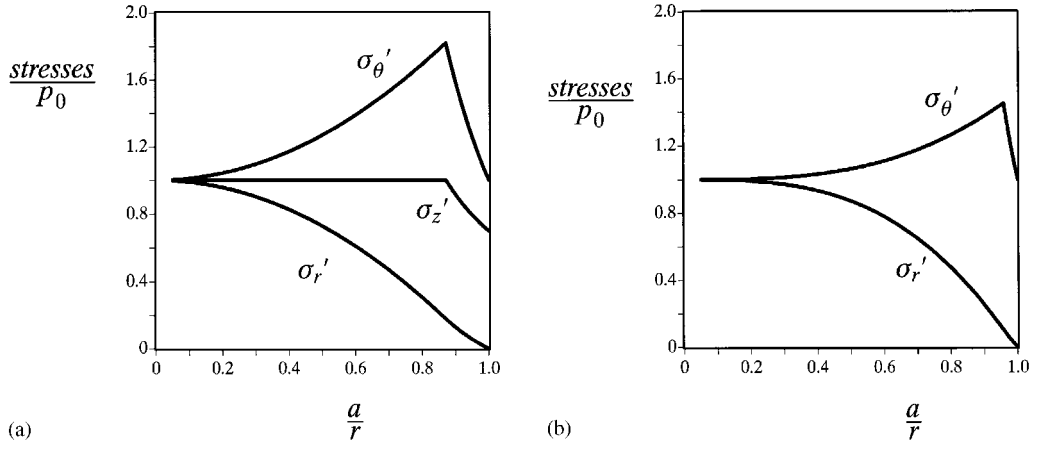

Figure 10. Effective stresses around tunnels in drained Mohr–Coulomb soils at complete unloading for $\phi = 40°$, $\psi = 20°$, $Y/p_0 = 1{\cdot}0$, $G/p_0 = 50$, (a) cylindrical cavity model; (b) spherical cavity model

Table I. Initial soil parameters for the analyses presented in Figures 11–18

Figure	k	s_u/p_0	G_0/s_u	n_p	Model
11	1	0·21	61·7	1·001	
	2	0·24	61·9	1·001	
12	1	0·32	40·3	2	Original
	2	0·37	40·5	2	Cam
13	1	0·56	22·9	5	Clay
	2	0·65	23·1	5	
14	1	0·86	15	10	
	2	0·99	15·1	10	
15	1	0·86	173·8	10	Hvorslev
	2	0·99	151·4	10	
16 and 18	1	0·25	51·1	1·001	Modified
	2	0·29	51·3	1·001	Cam
17	1	0·39	33·4	2	Clay
	2	0·44	33·5	2	

(b) The soil displacements induced by tunnelling from the plane strain cylindrical cavity theory is much larger (typically 3–5 times) than those from the spherical cavity theory.

(c) The cylindrical cavity theory predicts that, with the exception of normally consolidated clays (where large strain effects are very significant), the normalized displacement $-u/a$ varies linearly with a/r. Unlike fully drained cases, in undrained clays this is true in both elastic and plastic deforming regions.

(d) The soil displacements induced by tunnelling decrease with increasing value of the overconsolidation ratio n_p. This suggests that the overconsolidation ratio is an important parameter in the estimate of ground settlement due to tunnelling.

To study the effect of different yield surfaces on the predicted soil behaviour, heavily overconsolidated clays and normally consolidated clays are now modelled by the Hvorslev criterion and

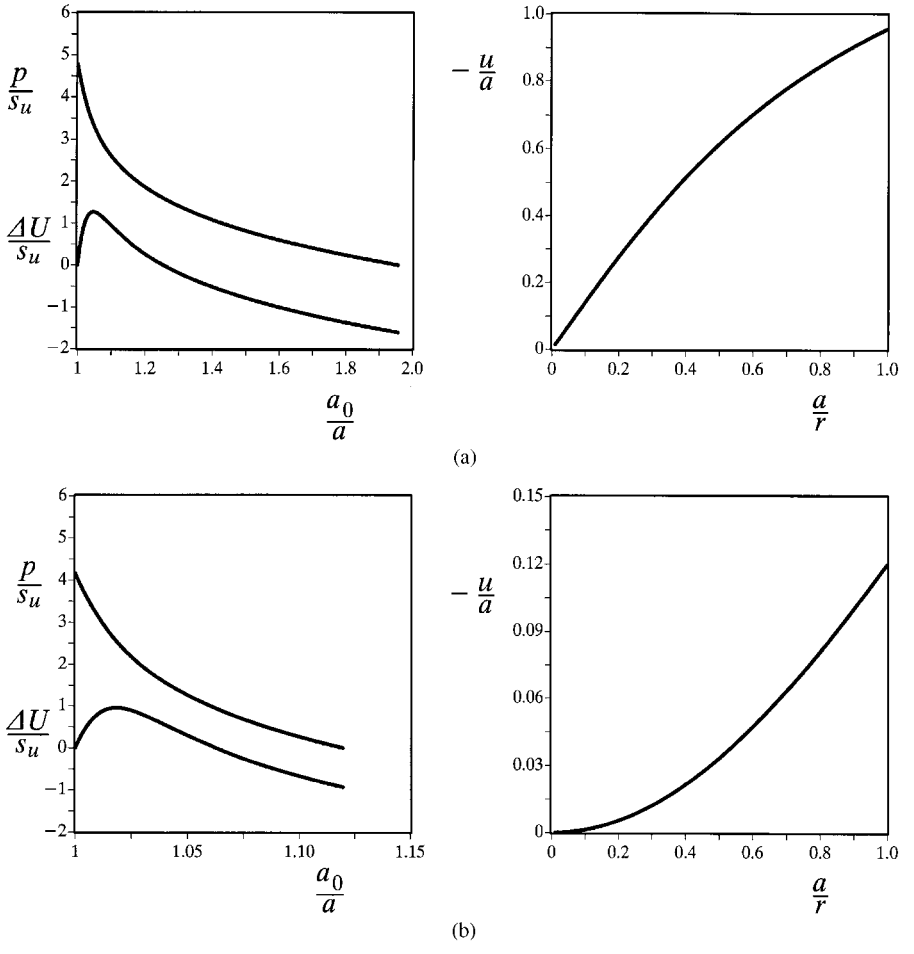

Figure 11. Large-strain solutions for soil behaviour around tunnels in original Cam clay with $n_p = 1{\cdot}001$, (a) cylindrical cavity model; (b) spherical cavity model

the modified Cam-Clay model, respectively. Selected results of the analyses with these new yield surfaces are plotted in Figures 15–17. By comparison, it is noted that the choice of a particular critical state model has a very important effect on the predicted soil behaviour around tunnels and this is particularly true for heavily overconsolidated clays. In general, the use of more realistic soil models such as the Hvorslev criterion for heavily overconsolidated clays and the modified Cam-Clay model for normally consolidated clays tends to predict smaller displacements around tunnels.

Presented in Figure 17 are the solutions of soil behaviour around tunnels in modified Cam clay with the overconsolidation ratio of 2. This corresponds to the special case when soil behaves as elastic perfectly plastic material. For this special case, it can be shown that the current solutions are identical to the conventional total stress solutions with the Tresca yield criterion. An example of the solutions for stress and pore pressure changes has been presented in Figure 18. The solutions presented are for normally consolidated clays modelled by the modified Cam-Clay

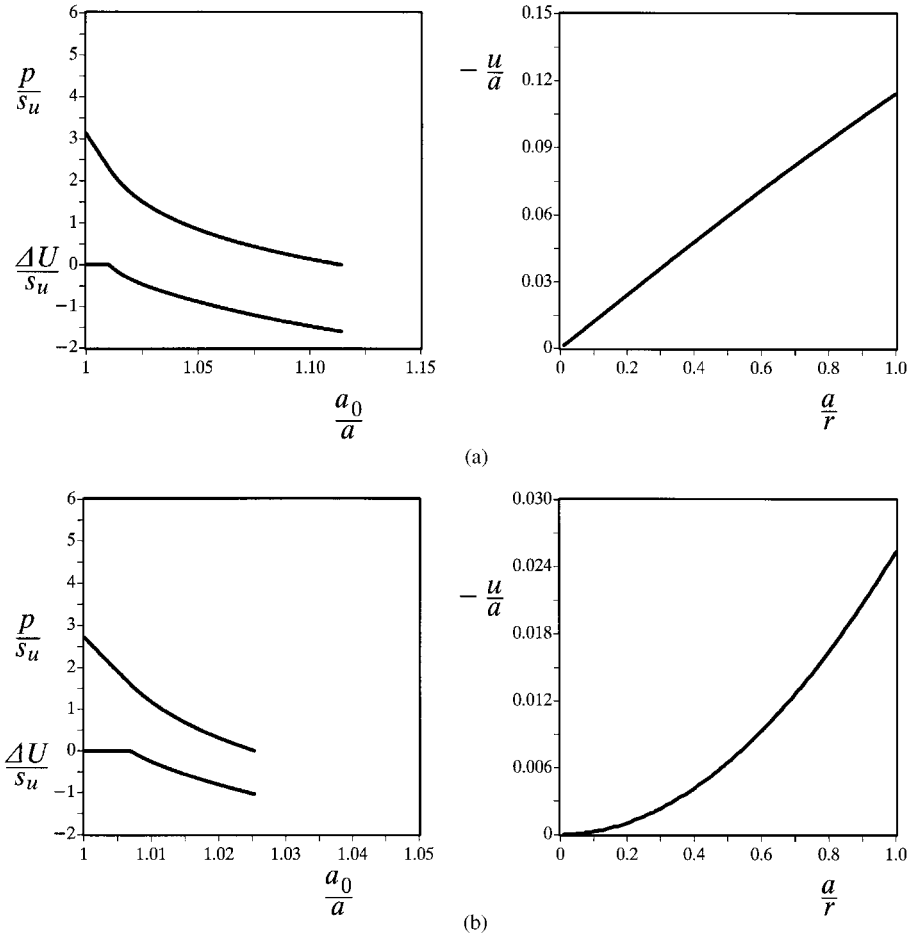

Figure 12. Large-strain solutions for soil behaviour around tunnels in original Cam clay with $n_p = 2{\cdot}0$, (a) cylindrical cavity model; (b) spherical cavity model

model. It is noted that the axis of radius is normalized by the radius of elastic–plastic interface R, and in this way the results presented in Figure 18 remain valid for any stage of elastic–plastic cavity unloading process.

COMPARISON WITH A CENTRIFUGE TUNNEL TEST IN CLAY

To demonstrate the relevance of the present cavity unloading solutions for modelling soil behaviour around tunnels, it is necessary to compare the predicted behaviour with quality experimental data. A comparison between the theoretical solutions and experimental results can give valuable insights on the applicability of the cavity unloading solutions to tunnel modelling.

In this section, we will show a comparison between predicted and observed crown and mid-surface settlements for a centrifuge tunnel test reported by Mair.[23] The tunnel test chosen for

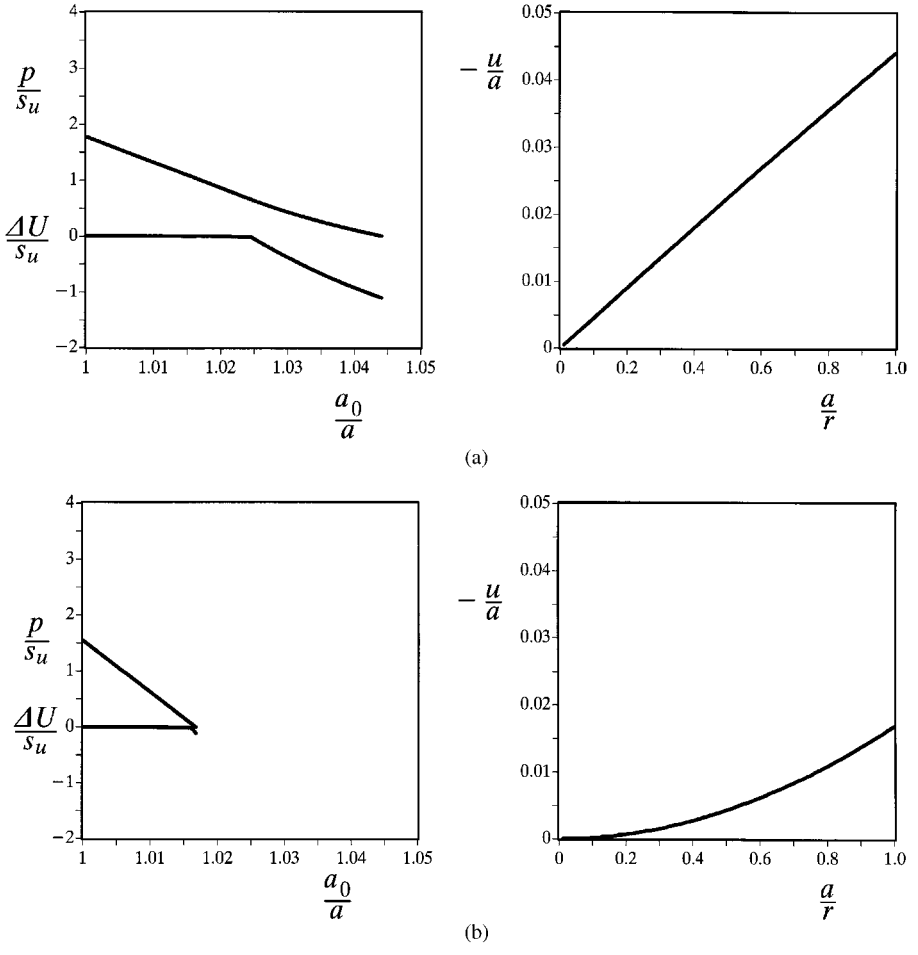

Figure 13. Large-strain solutions for soil behaviour around tunnels in original Cam clay with $n_p = 5{\cdot}0$, (a) cylindrical cavity model; (b) spherical cavity model

the comparison to test 2DP, which has a cover to diameter ratio of 1·67 (see Figure 19). The tunnel test was carried out quickly so that soil behaviour can be assumed to be undrained. The measured crown and mid-surface settlements for Test 2DP are presented in Figure 7.8 of Mair.[23] According to Mair, the critical state soil properties of the clay used for Test 2DP may be assumed to be $\Gamma = 3{\cdot}92$, $\lambda = 0{\cdot}3$, $\kappa = 0{\cdot}05$, $M = 0{\cdot}8$. The Poisson ratio is assumed to be 0.3. Although the clay around the tunnel in Test 2DP is lightly overconsolidated, the exact value of overconsolidation ratio in terms of mean effective stress, n_p, is not known. This is further complicated by the fact that the overconsolidation ratio n_p defined in terms of mean effective stress is variably greater than the one-dimensional overconsolidation ratio (OCR) defined in terms of vertical effective stress.[21] It is also not clear what was the specific volume of the clay before the tunnel test was carried out. As a result, some assumptions need to be made as to what values should be used for the initial specific volume and the overconsolidation ratio n_p. From the value of undrained shear

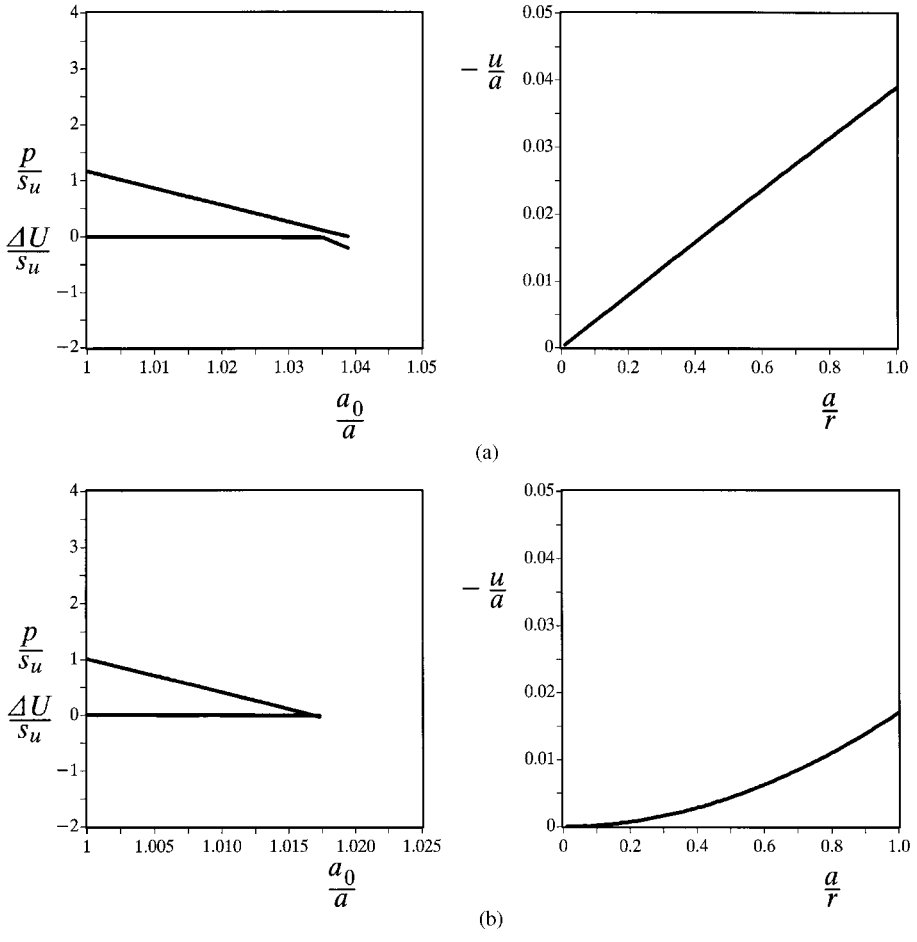

Figure 14. Large-strain solutions for soil behaviour around tunnels in original Cam clay with $n_p = 10{\cdot}0$, (a) cylindrical cavity model; (b) spherical cavity model

strength $s_u = 26$ kPa and $s_u = 0{\cdot}5M \exp((\Gamma - v)/\lambda)$, the initial specific volume may be estimated as $v = 2{\cdot}67$. After the specific volume is assumed, the overconsolidation ratio n_p is then estimated in such a way that the predicted initial tunnel support pressure is equal to that used in the centrifuge tunnel test.

Plotted in Figure 19 is a comparison between the predicted and observed crown and mid-surface settlements when the tunnel support pressure is reduced. The tunnel support pressure and settlements are normalized by undrained shear strength and initial tunnel radius, respectively. Although the predicted settlements shown in Figure 19 are obtained from cylindrical cavity unloading solution with the original Cam-Clay soil model, similar results can be obtained from other critical state models. The differences in prediction with different critical state models are not very significant for this particular case as the clay used in Test 2DP is only lightly overconsolidated.

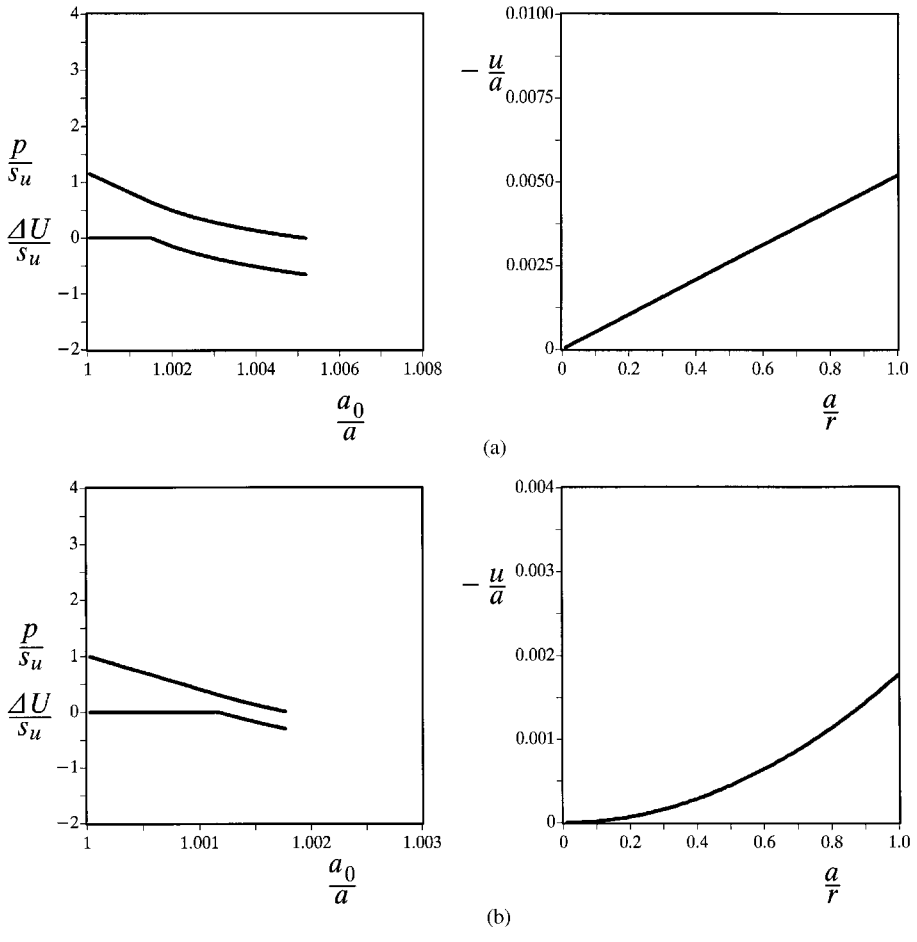

Figure 15. Large-strain solutions for soil behaviour around tunnels for the Hvorslev model with $n_p = 10.0$, (a) cylindrical cavity model; (b) spherical cavity model

From the comparison shown in Figure 19, it can be concluded that the present cavity unloading solutions can be used to accurately predict crown settlements around the tunnel. In contrast, the cavity unloading solutions tend to underpredict the observed mid-surface settlement. This is probably due to the fact that the model test 2DP is a shallow tunnel test with a very low cover to diameter ratio (1·67). For very shallow tunnels, solutions for contracting cavities in an infinite soil medium are expected to be less accurate for modelling the behaviour of soils far away from the cavity wall and this is due to the effect of free ground surface. For relatively deep tunnels, however, the present cavity unloading solutions could give more accurate predictions for surface settlements around the tunnel.

For comparison, the predicted crown and mid-surface settlements carried out by Mair[23] using a two-dimensional finite element model are also given in Figure 19. It is interesting to note that although the present cavity unloading solutions are very simple, they give similar predictions as

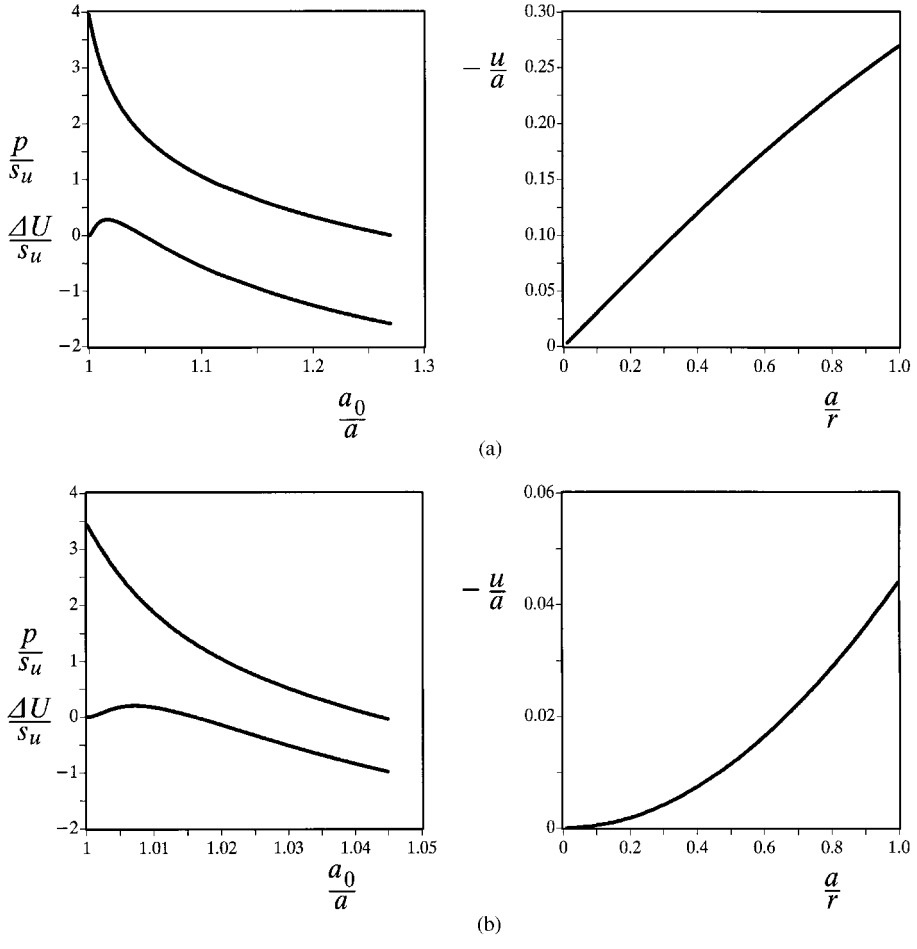

Figure 16. Large-strain solutions for soil behaviour around tunnels in modified Cam clay with $n_p = 1{\cdot}001$, (a) cylindrical cavity model; (b) spherical cavity model

those made by Cambridge's finite element program CRISP, which is known to be much more involved. This would suggest that the simple analytical solutions developed in this paper may have a useful role to play in the analysis and design of tunnels in soils.

CONCLUSION

This paper presents large strain analytical solutions of drained and undrained unloading of cylindrical and spherical cavities with a non-associated Mohr–Coulomb criterion and various critical state soil models. The solution procedure for the undrained case is applicable to any isotropically hardening materials. In all cases only simply quandratures are involved, but in the case of original Cam clay a complete analytical solution has been derived. It has also been shown that the well-known perfectly plastic solution can be recovered as a special case of the present

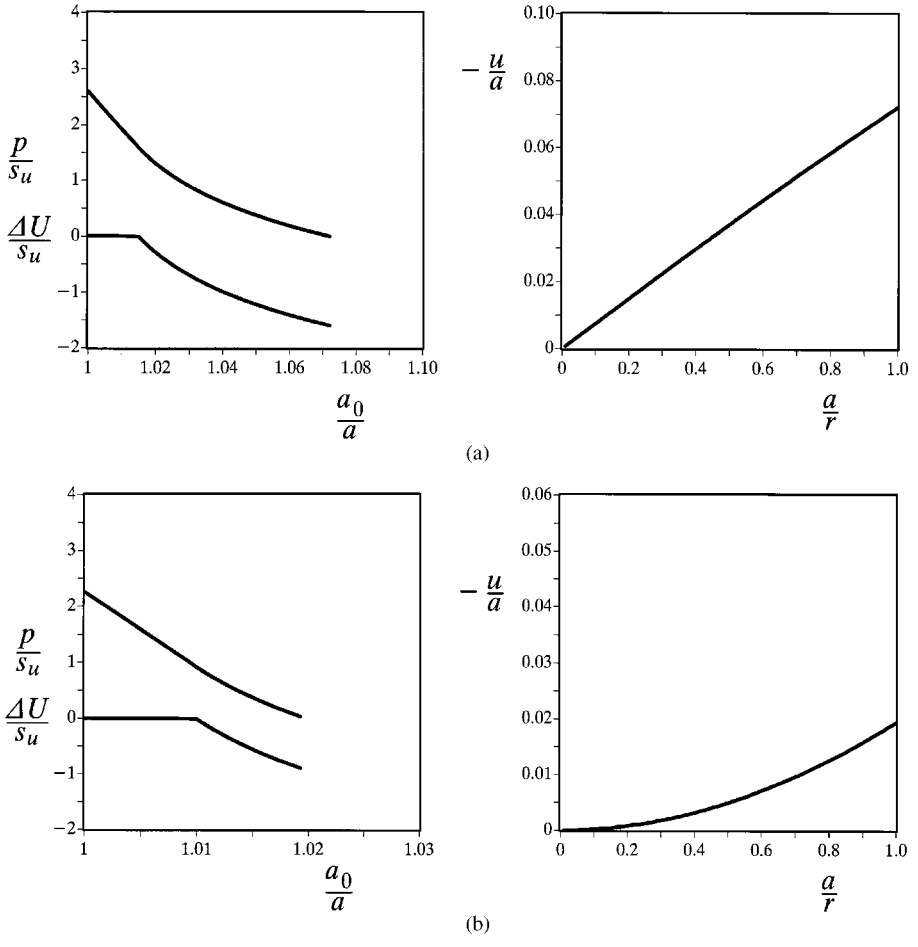

Figure 17. Large-strain solutions for soil behaviour around tunnels in modified Cam clay with $n_p = 2{\cdot}0$, (a) cylindrical cavity model; (b) spherical cavity model

undrained solution. The influence of the conventional small-strain assumption in the drained analysis, and the choice of various critical state models in the undrained analysis on the predicted soil behaviour around tunnels have been investigated in detail.

Using the results of a centrifuge tunnel test in clay, a comparison is made between the predicted and observed settlements around the tunnel. The results of this comparison suggest that the present simple cavity unloading solutions can be used to accurately predict the crown settlements. For a very shallow tunnel, the cavity unloading solutions tend to underpredict the observed mid-surface settlement. It is also noted that the predicted settlements made by the present simple cavity unloading solutions are similar to those predicted by the Cambridge finite element program, CRISP. The detailed comparison of the predicted soil behaviour around tunnels with field measurements is beyond the scope of this paper and will be presented in a future paper.

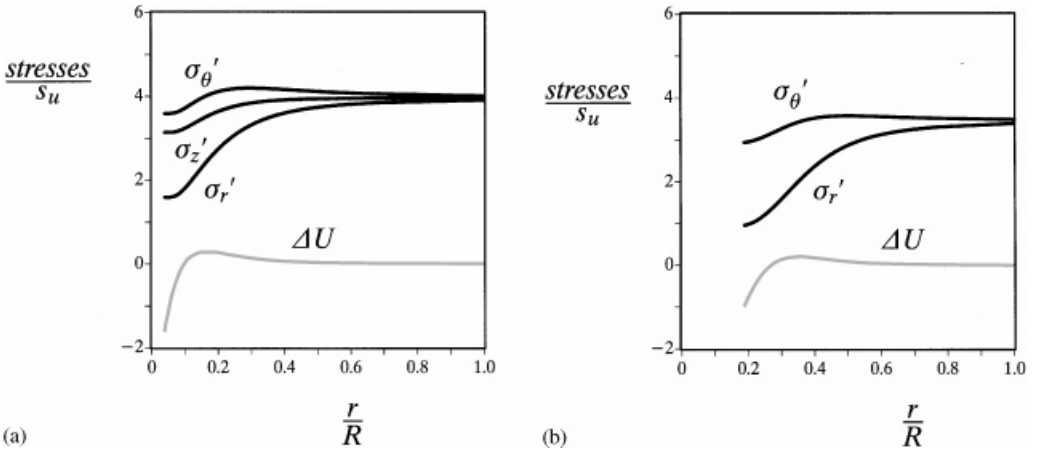

Figure 18. Effective stresses and pore pressure changes around tunnels in modified Cam clay with $n_p = 1{\cdot}001$, (a) cylindrical cavity model; (b) spherical cavity model

ACKNOWLEDGEMENTS

The work presented in this paper was carried out during the period of December 1996 to January 1997 when the first Author was a Visiting Professor at the University of Western Ontario, Canada. The first Author wishes to thank Professor I.F. Collins, University of Auckland, for providing many stimulating discussions on cavity expansion theory over the last few years.

APPENDIX A

This appendix derives the sufficient condition for the consistency of stress and strain assumptions in the axial direction of an unloading cylindrical cavity in the Mohr–Coulomb material.

The assumption of plane strain condition and the intermediacy of σ_z' results in two relationships between stresses in the plastic zone. First of all, the plane strain condition combined with the intermediacy of σ_z' gives

$$\dot{\varepsilon}_z^e = \frac{1}{E}[\dot{\sigma}_z' - \mu(\dot{\sigma}_r' + \dot{\sigma}_\theta')] = 0 \tag{86}$$

which can be integrated from the initial stress condition to give

$$\frac{\sigma_z'}{p_0} = 1 + \mu\left(\frac{\sigma_r'}{p_0} + \frac{\sigma_\theta'}{p_0} - 2\right) \tag{87}$$

Secondly, the assumption of the intermediacy of σ_z' gives the yield function (10) which can be further written as

$$\frac{\sigma_\theta'}{p_0} = \alpha\frac{\sigma_r'}{p_0} + \frac{Y}{p_0} \tag{88}$$

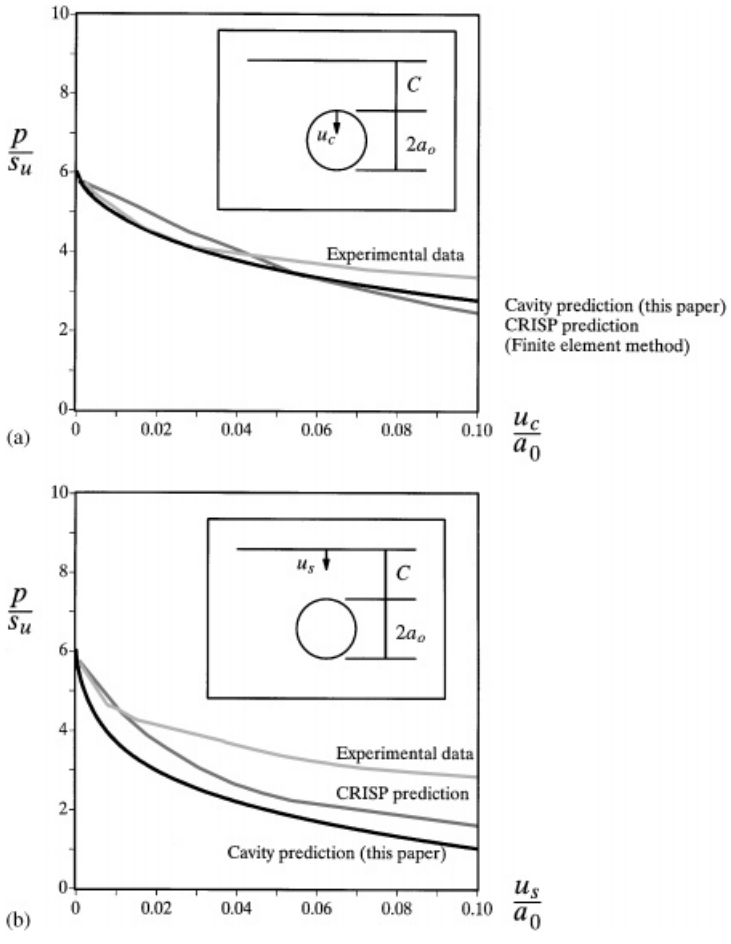

Figure 19. Comparison between predicted (using cylindrical cavity solutions) and observed settlements for a centrifuge tunnel test in clay (Test 2DP reported in Mair[23] with a cover to diamater ratio of $C/2a_0 = 1{\cdot}67$), (a) predicted and observed crown settlements as tunnel pressure is reduced; (b) predicted and observed mid-surface settlements as tunnel pressure is reduced

Substituting equation (88) into (89) leads to

$$\frac{\sigma'_z}{p_0} = 1 + \mu\left[\frac{\sigma'_r}{p_0}(1+\alpha) + \frac{Y}{p_0} - 2\right] \tag{89}$$

During the unloading of a cavity, the radial stress decreases while the hoop and the axial stresses tend to increase. To ensure that the axial stress remains as the intermediate stress, it is sufficient to impose the following condition:

$$\frac{\sigma'_z}{p_0} \leqslant \frac{\sigma'_\theta}{p_0} \tag{90}$$

Using equations (88) and (89), the above condition can be expressed as

$$\frac{1-\mu}{1-2\mu}\frac{Y}{p_0}+\frac{\alpha-\mu(1+\alpha)}{1-2\mu}\frac{\sigma_r'}{p_0}\geqslant 1 \tag{91}$$

Because violation of the above condition would occur first at the cavity wall, and to avoid such a violation it is sufficient to satisfy the condition at the cavity wall:

$$\frac{1-\mu}{1-2\mu}\frac{Y}{p_0}+\frac{\alpha-\mu(1+\alpha)}{1-2\mu}\frac{p}{p_0}\geqslant 1 \tag{92}$$

APPENDIX B: NOTATION

A	constant
a	current radius of cavity wall
a_0	initial radius of cavity wall
B	constant
c	soil cohesion
E	Young's modulus
e	superscript to indicate elastic component, and the natural base of logarithm (= 2.7182)
ε_r	radial strain rate
ε_θ	hoop strain rate
f, g	functions of effective mean stress
G	shear modulus
G_0	initial shear modulus
I	function of effective mean stress
J	function of finite shear strain
k	cavity type indicator
K_0	initial bulk modulus
$K_{\max}$	maximum bulk modulus
L	function of effective mean stress
m	function of Young's modulus and Poisson's ratio
N	specific volume on the normal consolidation line
n_p	overconsolidation ratio in terms of mean effective stress
p	superscript to indicate plastic component or tunnel support pressure
p'	effective mean stress
p_e'	equivalent consolidation pressure
$\bar{p}'$	normalized effective mean stress
q	effective shear stress
$\bar{q}$	normalized effective shear stress
R	current radius of elastic–plastic boundary
r	current radius of a material element
r_0	initial radius of a material element
s_u	triaxial undrained shear strength
u	soil displacement
u_c	crown settlement of a tunnel (see Figure 19)

u_s mid-surface settlement of a tunnel (see Figure 19)
U pore water pressure
ΔU excess pore water pressure
$\bar{U}$ normalized pore water pressure
$\Delta \bar{U}$ normalized excess pore water pressure
v soil specific volume
w speed of cavity expansion
μ Poisson's ratio
λ slope of the normal consolidation line
κ slope of elastic swelling line
Λ $\dfrac{\lambda - \kappa}{\lambda}$
Γ specific volume of a point in critical state line corresponding to $p' = 1$ kPa
γ finite shear strain
γ_c finite shear strain at cavity wall
$\dot{\gamma}$ shear strain rate
δ volumetric strain
$\dot{\delta}$ volumetric strain rate
σ'_r effective radial stress
σ'_z effective axial stress for cylindrical cavity
σ'_θ effective hoop stress
ϕ angle of soil friction
ϕ_{cs} critical state angle of soil friction
ϕ_{hc} soil friction angle defined by the Hvorslev yield surface
ψ angle of soil dilation
α function of soil friction
β function of soil dilation

$h = \dfrac{6 \sin \phi_{hc}}{3 - \sin \phi_{hc}}$ for spherical cavity; and $h = 2 \sin \phi_{hc}$ for cylindrical cavity

$M = \dfrac{6 \sin \phi_{cs}}{3 - \sin \phi_{cs}}$ for spherical cavity; and $M = 2 \sin \phi_{cs}$ for cylindrical cavity

$Y = \dfrac{2c \cos \phi}{1 - \sin \phi}$

REFERENCES

1. E. T. Brown, J. W. Bray, B. Ladanyi and E. Hoek, 'Ground response curves for rock tunnels', ASCE, *J. Geotech. Engng*., **109**(1), 15–39 (1983).
2. K. Y. Lo, M. C. Ng and R. K. Rowe, 'Predicting settlement due to tunnelling in clays', *Tunnelling in Soil and Rock*, *ASCE Geotech III Conf*., Atlanta, GA, 1984, pp. 48–76.
3. T. Ogawa and K. Y. Lo, 'Effects of dilatancy and yield criteria on displacements around tunnels, *Can. Geotech. J*., **24,** 100–113 (1987).
4. R. J. Mair and R. N. Taylor, 'Prediction of clay behavior around tunnels using plasticity solutions', *Proc. Peter Wroth Memorial Symp*., Predictive Soil Mechanics, 1993, pp. 449–463.
5. R. K. Rowe and G. J. Kack, 'A theoretical examination of the settlements induced by tunnelling: four case histories, *Can. Geotech. J*., **20**(2), 299–314 (1983).
6. M. F. Randolph, J. P. Carter and C. P. Worth, 'Driven piles in clay — the effects of installation and Subsequent consolidation', *Geotechnique*, **29,** 361–393 (1979).

7. I. F. Collins and H. S. Yu, 'Undrained cavity expansions in critical state soils', *Int. J. Numer. Anal. Meth. Geomech.*, **20,** 485–516 (1996).
8. C. Sagaseta, 'Analysis of undrained soil deformation due to ground loss', *Geotechnique*, **37**(3)**,** 301–320 (1987).
9. R. K. Rowe, 'The prediction of deformations caused by soft ground tunnelling—recent trends', In D. Eisenstein (ed.), *Canadian Tunnelling*. 1986, pp. 91–108.
10. H. S. Yu and G. T. Houlsby, 'Finite cavity expansion in dilatant soil: loading analysis', *Geotechnique*, **41,** 173–183 (1991).
11. J. P. Carter, J. R. Booker and S. K. Yeung, 'Cavity expansion in cohesive-frictional soils', *Geotechnique* **36,** 349–358 (1986).
12. H. S.Yu and G. T. Houlsby, 'A large strain analytical solution for cavity contraction in dilatant soils', *Int. J. Numer. Anal. Mech. Geomech.*, **19,** 793–811 (1995).
13. M. B. Reed, 'The influence of out-of-plane stress on a plane strain problem in rock mechanics', *Int. J. Numer. Anal. Meth. Geomech.*, **12,** 173–181 (1988).
14. E. H. Davis, 'Theories of plasticity and the failure of soil masses', in I. K. Lee (ed.), *Soil Mechanics: Selected Topics*, Butterworths, Sydney.
15. H. S. Yu, 'Interpretation of pressuremeter unloading tests in sands', *Geotechnique*, **46,** 17–34 (1996).
16. A. N. Schofield and C. P. Worth, *Critical State Soil Mechanics*, McGraw-Hill, New York, 1968.
17. A. Gens and D. M. Potts, 'Critical state models in computational geomechanics', *Engng. Comput.* **5,** 178–197 (1988).
18. J. H. Atkinson and P. L. Bransby, *The Mechanics of Soils*, McGraw-Hill, New York, 1978.
19. D. Sheng, S. W. Sloan and H. S. Yu, 'Practical implementation of critical state models in FEM', *Proc. 8th Australia New Zealand Conf. on Geomechanics*, Hobart, Australia, Vol. 2, 1999.
20. M. Zytynski, M. F. Randolph, R. Nova and C. P. Wroth, 'On modelling the unloading-reloading behaviour of soils', *Int. J. Numer. Anal. Meth. Geomech.*, **2,** 87–93 (1978).
21. K. H. Roscoe and J. B. Burland, 'On the generalized stress-strain behaviour of wet clay', *Engineering Plasticity*, Cambridge University Press, Cambridge, 1968, pp. 535–609.
22. D. Muir Wood, *Soil Behaviour and Critical State Soil Mechanics*, Cambridge University Press, Cambridge, 1990.
23. R. J. Mair, Centrifuge modelling of tunnel construction in soft clay, *Ph.D. Thesis*, University of Cambridge, 1979.

